Crystal Structures of the Binary and Ternary Complexes of 7α-Hydroxysteroid Dehydrogenase from *Escherichia coli*[†,‡]

Nobutada Tanaka,[§] Takamasa Nonaka,[§] Tetsurou Tanabe,[∥] Tadashi Yoshimoto,[∥] Daisuke Tsuru,[⊥] and Yukio Mitsui*[,§]

Department of BioEngineering, Nagaoka University of Technology, Kamitomioka, Nagaoka, Niigata 940-21, Japan, School of Pharmaceutical Sciences, Nagasaki University, Bunkyo-machi, Nagasaki, Nagasaki 852, Japan, and Department of Applied Microbial Technology, Kumamoto Institute of Technology, Ikeda, Kumamoto, Kumamoto 860, Japan

Received August 14, 1995; Revised Manuscript Received March 29, 1996[⊗]

ABSTRACT: 7α-Hydroxysteroid dehydrogenase (7α-HSDH;[1] EC 1.1.1.159) is an NAD^+-dependent oxidoreductase belonging to the short-chain dehydrogenase/reductase (SDR)[1] family. It catalyzes the dehydrogenation of a hydroxyl group at position 7 of the steroid skeleton of bile acids. The crystal structure of the binary (complexed with NAD^+) complex of 7α-HSDH has been solved at 2.3 Å resolution by the multiple isomorphous replacement method. The structure of the ternary complex [the enzyme complexed with NADH, 7-oxoglycochenodeoxycholic acid (as a reaction product), and possibly partially glycochenodeoxycholic acid (as a substrate)] has been determined by a difference Fourier method at 1.8 Å resolution. The enzyme 7α-HSDH is an α/β doubly wound protein having a Rossmann-fold domain for NAD(H) binding. Upon substrate binding, large conformation changes occur at the substrate binding loop (between the βF strand and the αG helix) and the C-terminal segment (residues 250−255). The variable amino acid sequences of the substrate-binding loop appear to be responsible for the wide variety of substrate specificities observed among the enzymes of the SDR family. The crystal structure of the ternary complex of 7α-HSDH, which is the only structure available as the ternary complex among the enzymes of the SDR family, indicates that the highly conserved Tyr159 and Ser146 residues most probably directly interact with the hydroxyl group of the substrates although this observation cannot be definite due to an insufficiently characterized nature of the ternary complex. The strictly conserved Lys163 is hydrogen-bonded to both the 2′- and 3′-hydroxyl groups of the nicotinamide ribose of NAD(H). We propose a new catalytic mechanism possibly common to all the enzymes belonging to the SDR family in which a tyrosine residue (Tyr159) acts as a catalytic base and a serine residue (Ser146) plays a subsidiary role of stabilizing substrate binding.

In humans, two major bile acids, together termed primary bile acids, are formed from cholesterol in the liver. They are cholic acid and chenodeoxycholic acid. The glycine and taurine conjugates of primary bile acids are modified by intestinal flora. The predominant modifications include deconjugations of glycine and taurine moieties, removal of a hydroxyl group at position 7 of the steroid skeleton, and dehydrogenation of the hydroxyl groups at positions 3, 7, and 12 of the steroid skeleton by stereospecific bile acid hydroxysteroid dehydrogenase (HSDH)[1] to yield oxo bile acids. The major reaction of physiological significance is the 7α-dehydroxylation of cholic and chenodeoxycholic acids, producing deoxycholic and lithocholic acids, respectively. Microbial stereospecific dehydrogenation has been reported for the hydroxyl groups at positions 3, 6, 7, and 12 of the steroid skeleton of bile acids in both the α and β orientations. In human intestinal flora, 7α-HSDH is much more abundant than 3α-HSDH or 12α-HSDH. 7α-HSDH has been detected in numerous genera of bacteria and in mammalian livers. Thus purifications of 7α-HSDH have been reported for *Escherichia coli* (Macdonald et al., 1973; Prabha et al., 1989, 1990), *Bacteroides* species (Macdonald et al., 1975; Hylemon & Sherrod, 1975, 1977; Franklund et al., 1990), and rat liver microsomes (Amuro et al., 1987). Recently, two 7α-HSDH's have been cloned, sequenced, and characterized. One is an NAD-linked enzyme from *E. coli* HB101 (Yoshimoto et al., 1991, 1993) and the other is an NADP-linked enzyme from the *Eubacterium* sp. strain VPI12708 (Baron et al., 1991). These two 7α-HSDH's have similar subunit compositions, molecular weights, and substrate specificities. The deduced amino acid sequences of these enzymes show that they belong to the short-chain (see below for definition) dehydrogenase/reductase (SDR) family (Yoshimoto et al., 1991; Baron et al., 1991).

[†] This work was supported, in part, by grants from the Ministry of Education, Science and Culture, Japan, given to Y.M. and from the Sakabe project of the TARA (Tsukuba Advanced Research Alliance) center at the University of Tsukuba. N.T. is supported by a fellowship from the Japan Society for the Promotion of Science.

[‡] Crystallographic coordinates for the binary complex of 7α-HSDH have been deposited with the Brookhaven Protein Data Bank as entry 1AHH and those for the ternary complexes of 7α-HSDH as entries 1AHI and 1FMC.

* To whom correspondence should be addressed.

[§] Department of BioEngineering, Nagaoka University of Technology.

[∥] School of Pharmaceutical Sciences, Nagasaki University.

[⊥] Department of Applied Microbial Technology, Kumamoto Institute of Technology.

[⊗] Abstract published in *Advance ACS Abstracts,* May 15, 1996.

[1] Abbreviations: DADH, *Drosophila* alcohol dehydrogenase; DHPR, dihydropteridine reductase; GCDCA, glycochenodeoxycholic acid; 3α,-20β-HSDH, 3α,20β-hydroxysteroid dehydrogenase; 7α-HSDH, 7α-hydroxysteroid dehydrogenase; 17β-HSDH, 17β-hydroxysteroid dehydrogenase; MIR, multiple isomorphous replacement; rms, root mean square; SDR, short-chain dehydrogenases/reductases; SIR, single isomorphous replacement.

S0006-2960(95)01904-0 CCC: $12.00

The dehydrogenase superfamily has been divided into three families: the long-chain, medium-chain, and short-chain families (Persson et al., 1991). The long-chain family has not been well characterized (Inoue et al., 1989). The medium-chain family, such as alcohol dehydrogenase, lactate dehydrogenase, soluble malate dehydrogenase, and glyceraldehyde-3-phosphate dehydrogenase, is well characterized at the level of three-dimensional structure [reviewed in Rossmann et al. (1975)]. These enzymes use NAD(H) or NADP(H) as cofactors and are either dimeric or tetrameric in the active state. Each monomer contains typically 350−400 amino acid residues and is composed of two domains, the catalytic domain and the coenzyme-binding domain. All of the coenzyme-binding domain elucidated for this family of enzymes has a common $\beta\alpha\beta$ supersecondary structure called the Rossmann fold while the structures of the catalytic domain are varied among these enzymes (Rossmann et al., 1975). Investigations of the short-chain dehydrogenase family started only in the 1980s (Jörnvall et al., 1981, 1984), and more than 50 different enzymes have been characterized as belonging to the short-chain dehydrogenase/reductase (SDR) family (Jörnvall et al., 1995). The enzymes belonging to the short-chain family (hereafter the short-chain enzymes) exhibit a wide variety of substrate specificities for alcohol, ribitol, glucose, 15-hydroxyprostaglandin, several hydroxysteroids, and so forth. Like the medium-chain enzymes, the short-chain enzymes are either dimers or tetramers and use NAD(H) or NADP(H) as cofactors. However, unlike the medium-chain enzymes, no zinc atoms are bound to these enzymes. Each monomer contains typically 250 residues. The coenzyme-binding domain is located in the N-terminal side of the protein, and the catalytic domain is located toward the C-terminus of the protein (Persson et al., 1991). To date, three-dimensional structures have been elucidated only for three enzymes of this family: 3α,20β-hydroxysteroid dehydrogenase (3α,20β-HSDH)[1] at 2.6 Å resolution [binary complex with NADH (Ghosh et al., 1991, 1994a)], dihydropteridine reductase (DHPR)[1] at 2.3 Å resolution [binary complex with NADH (Varughese et al., 1992)], and 17β-hydroxysteroid dehydrogenase (17β-HSDH)[1] at 2.2 Å resolution [apparently in apo form (Ghosh et al., 1995)]. Despite only up to 15% sequence identities, the three-dimensional structures of these enzymes turned out to be basically identical among the three short-chain enzymes. The crystal structures of these enzymes revealed that their coenzyme-binding domains commonly have the Rossmann-fold structure as found in the medium-chain enzymes. The postulated active sites are composed of several conserved amino acid residues and the nicotinamide moieties of the coenzyme NAD(H). Multiple alignment of amino acid sequences for the enzymes of the short-chain dehydrogenase/reductase family revealed that only the amino acid residues in the coenzyme-binding domain and postulated active site are highly conserved (Varughese et al., 1994). Recently, Ghosh et al. solved the crystal structure of 3α,20β-HSDH complexed with carbenoxolone as an inhibitor at 2.2 Å resolution (Ghosh et al., 1994b). In this structure, however, no bound coenzyme was found. Thus it cannot be regarded as representing the structure of the productive ternary complex although it did show that a side chain of the inhibitor molecule forms a hydrogen bond with the hydroxyl group of an evolutionarily strictly conserved tyrosine residue.

In order to understand the possibly common catalytic mechanism shared by the enzymes belonging to the SDR family (the short-chain enzymes) and the origin of a wide variety of substrate specificities observed among these enzymes, we have begun crystallographic studies on 7α-hydroxysteroid dehydrogenase (7α-HSDH) from *E. coli*. Here we report on the crystal structures of the binary (complexed with NAD^+) complex of 7α-HSDH (or holo-7α-HSDH) at 2.3 Å resolution and a ternary complex of 7α-HSDH [complexed with NADH, 7-oxoglycochenodeoxycholic acid (as a reaction product), and possibly partially glycochenodeoxycholic acid (as a substrate)] at 1.8 Å resolution. This is the first crystal structure of the ternary complex of a short-chain enzyme although the nature of the molecular species present in the ternary complex has not yet been fully characterized. We will show the occurrence of large conformation changes upon substrate binding and evidence that the side chains of a tyrosine and a serine residue, which are evolutionarily conserved, most probably, directly interact with the substrate. Observation of these features may permit detailed description as to the origins of a wide variety of substrate specificities observed among the enzymes belonging to the SDR family and the possibly common catalytic mechanism shared by these short-chain enzymes.

MATERIALS AND METHODS

Preparation of the Binary Complex Crystals and Heavy-Atom Derivatives. 7α-HSDH was purified as described before (Yoshimoto et al., 1991). Crystals of the binary (complexed with NAD^+) complex of 7α-HSDH (or holo-7α-HSDH) (hereafter to be called native crystal) were obtained by the hanging drop vapor diffusion method as described by Tanaka et al. (1996a). The crystals belong to a tetragonal space group $P4_12_12$ (the other possible space group, $P4_32_12$, was excluded as described below) with cell dimensions of $a = b = 81.66$ Å and $c = 214.6$ Å. Assuming two subunits per asymmetric unit, this leads to a V_m value of 3.34 Å^3/Da, corresponding to a solvent content of 63% (Matthews, 1968). Three heavy-atom derivatives were prepared by transferring native crystals first into the standard solution (buffered at pH 8.5 by 100 mM Tris) containing 30% (w/v) PEG 6000, 200 mM sodium acetate, and 2.8 mM NAD^+. Such crystals were then transferred into a series of derivative solutions containing 0.1 mM $HgCl_2$, 2 mM K_2PtCl_4, or 1 mM $KAu(CN)_2$ dissolved into the standard solution.

Preparation of the Ternary Complex Crystals. To obtain the ternary complex crystals (intended to contain NADH and a substrate/product), the above-mentioned tetragonal crystals were soaked for 2 days at 20 °C in the substrate solution [buffered by 100 mM Tris at pH 8.5 (which is the optimum pH for 7α-HSDH)] containing 30% (w/v) PEG 6000, 200 mM sodium acetate, 2.8 mM NAD^+, and 5 mM glycochenodeoxycholic acid (GCDCA;[1] the chemical structure is given in Figure 1) as substrate. The substrate, GCDCA, rather than the product, 7-oxo-GCDCA, was used because only a minute amount of the latter compound, which was a gift from a laboratory at Tottori University (Japan), was available to us. Occurrence of the relevant reaction in these crystals was confirmed spectrophotometrically by monitoring the NADH production at 340 nm with a Shimadzu spectrometer (Model UV-1200). Thus the resultant crystals must contain the

Table 1: Data Collection Statistics for Crystals of the Binary Complex of 7α-HSDH (or Holo-7α-HSDH) (Denoted Native), Heavy-Atom Derivatives, and a Crystal Soaked in GCDCA[a] (Ternary Complex) (Denoted GCDCA)

data set (method)[b]	soaking conditions: concn (mM)	soaking conditions: time (days)	resolution (Å)	no. of reflections: obsd	no. of reflections: unique	completeness (%) (outer shell)	$R_{merge}(I)$[c] (%) (outer shell)	no. of crystals used
native (R-AXIS IIc)			2.30	79 500	28 146	84.6 (62.7)[d]	7.29 (24.2)[d]	1
$HgCl_2$ (R-AXIS IIc)	0.1	10	2.80	50 703	17 090	91.6	7.28	1
K_2PtCl_4 (R-AXIS IIc)	2	8	2.82	39 912	15 754	85.7	8.52	1
$KAu(CN)_2$ (R-AXIS IIc)	1	7	2.81	49 995	16 818	91.2	7.24	1
GCDCA[a] (R-AXIS IIc)	5	2	2.30	86 785	28 878	86.9 (64.6)[d]	8.87 (26.3)[d]	1
GCDCA[a] (PF)	5	2	1.80	221 323	57 290	84.4 (66.1)[e]	8.50 (39.7)[e]	1

[a] GCDCA: glycochenodeoxycholic acid (as a substrate). [b] Data were collected either by using the macromolecule-oriented Weissenberg camera at the Photon Factory (PF),Tsukuba (synchrotron data), or by using the R-AXIS IIc oscillation-type diffractometer in the present laboratory (laboratory data). [c] $R_{merge}(I) = \Sigma_h\Sigma_i|I_{(h)i} - \langle I_{(h)}\rangle|/\Sigma_h\Sigma_i I_{(h)i}$, where i represents different observations. [d] For the 2.40−2.30 Å shell. [e] For the 1.85−1.80 Å shell.

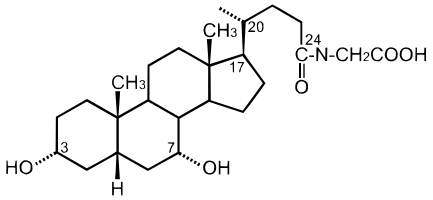

FIGURE 1: Structural formula for glycochenodeoxycholic acid (GCDCA) as a substrate for 7α-HSDH. The compound is conjugated by a glycine residue at position 24. Similar compounds with different conjugation patterns are known (see Discussion).

ternary complex of 7α-HSDH complexed with NADH, 7-oxo-GCDCA (as a reaction product), and possibly partially GCDCA (as a substrate). For details of this point, see the sections The Oxidation State of the Cofactor and The Oxidation State of the Substrate in Results.

X-ray Data Collection and Processing. Before X-ray data collection, crystals of the binary complex of 7α-HSDH (or holo-7α-HSDH) were transferred from hanging drops into the freshly prepared standard solution as described above. X-ray data collection was performed by an oscillation method at 20 °C using a Rigaku R-AXIS IIc area detector with Cu Kα radiation, which was generated by a Rigaku RU200 rotating-anode X-ray generator (operated at 45 kV and 110 mA), and focused by a Supper double focusing mirror. The best native X-ray data set was collected up to 2.3 Å resolution from a single crystal. The data for heavy-atom derivative crystals of the binary complex and the ternary complex crystal were respectively collected up to 2.8 and 2.3 Å resolution in a similar way. Each data set was processed with the program PROCESS installed in the R-AXIS IIc system and reduced with the CCP4 suite (Collaborative Computational Project, Number 4, 1994).

Finally, high-resolution data (1.8 Å) for the ternary complex crystal were collected at 15 °C ($\lambda = 1.00$) using a macromolecule-oriented Weissenberg camera devised by Prof. N. Sakabe (Sakabe et al., 1995), installed at BL18B of the Photon Factory synchrotron radiation source in Tsukuba, Japan. The synchrotron data were processed essentially in the same way as described by Takeuchi et al. (1991) using the program WEIS (Higashi, 1989). Hereafter, the data collected by a Rigaku R-AXIS IIc area detector as described above may sometimes be called laboratory data (as in Table 4).

The statistics for the native and derivative data sets are summarized in Table 1.

Structure Determination. Initially, we tried to solve the structure of 7α-HSDH by molecular replacement techniques.

Table 2: MIR Phasing Statistics for the Binary Complex of 7α-HSDH (or Holo-7α-HSDH)[a]

derivative	resolution (Å)	R_{iso} (%)[b]	no. of heavy-atom sites	R_{Cullis}[c]	phasing power[d]
$HgCl_2$	2.8	18.0	4	0.49	1.3
K_2PtCl_4	3.5	17.0	4	0.62	0.9
$KAu(CN)_2$	3.5	7.7	2	0.74	0.6

[a] Mean figure of merit (centric) = 0.714 at 2.8 Å resolution. [b] $R_{iso} = \Sigma_h|F_{(deriv)} - F_{(native)}|/\Sigma_h F_{(native)}$. [c] $R_{Cullis} = \Sigma_h||F_{(deriv)} \pm F_{(native)}| - F_{H(calc)}|/\Sigma_h|F_{(deriv)} \pm F_{(native)}|$ for centric reflections only. [d] Phasing power $= [\Sigma_h|F_H|^2/\Sigma_h\{|F_{(deriv)}| - |F_{(native)} + F_{H(calc)}|\}^2]^{1/2}$.

The structure of holo-3α,20β-HSDH (Ghosh et al., 1991, 1994a), having *ca.* 30% sequence identity with 7α-HSDH, was used as a search model. This attempt failed because we could not find any significant peak in translation search (although several weak peaks were found in rotation search). Thus the structure was determined by the multiple isomorphous replacement (MIR)[1] method using three heavy-atom derivatives. Two major mercury sites were determined by inspection of difference Patterson maps calculated with the shell X-ray data between 10 and 4 Å resolution. Program RSPS (Knight, 1989) was also used to determine the heavy-atom sites. Single isomorphous replacement (SIR)[1] phases based on a single mercury site were used to locate the minor sites and the sites in other derivatives through (cross) difference Fourier syntheses. The two sites in the $KAu(CN)_2$ derivative clearly appeared in such a map and turned out to be consistent with the peaks that appeared in the (self) difference Patterson map calculated for this derivative. Rather surprisingly, the latter Patterson map showed a set of very clear peaks despite the very low R_{iso} value (7.7%) for these data (see Table 2). Heavy-atom parameters were refined with the program MLPHARE (Otwinoski, 1991). The figure-of-merit for the refined phases was 0.71 for centric reflections to 2.8 Å resolution. The MIR phasing statistics and refined heavy-atom parameters are summarized in Tables 2 and 3, respectively. As usual, the space group ambiguity ($P4_12_12$ or $P4_32_12$) was resolved by incorporating anomalous data from the $HgCl_2$ derivative for phasing. The anomalous data, however, were not included in the final phase calculation. The MIR phases at 2.8 Å resolution were improved by solvent-flattening and histogram-matching algorithms and extended to 2.3 Å resolution using the program SQUASH (MIR-SQ) (Zhang & Main, 1990; Zhang, 1993). In order to prevent the loss of surface information, a value (40%) considerably lower than the experimentally estimated value

Table 3: Refined Heavy-Atom Parameters for the Binary Complex of 7α-HSDH (or Holo-7α-HSDH)

derivative	binding site	*x*	*y*	*z*	*B* (Å^2)	relative occupancy
$HgCl_2$	Cys13 (subunit 1)	0.491	0.004	0.101	62.6	1.02
	Cys65 (subunit 1)	0.637	0.036	0.041	63.6	0.35
	Cys13 (subunit 2)	0.441	0.371	−0.163	60.4	1.02
	Cys65 (subunit 2)	0.468	0.159	−0.145	58.9	0.70
K_2PtCl_4	Met1 (subunit 1)	0.270	0.179	0.152	80.0	0.44
	Met156 (subunit 1)	0.541	0.353	−0.007	111.0	0.96
	Met1 (subunit 2)	0.254	0.596	−0.121	79.1	0.86
	Met156 (subunit 1)	0.272	0.124	−0.032	89.5	0.84
$KAu(CN)_2$	Cys13 (subunit 1)	0.516	0.014	0.106	60.4	0.32
	Cys13 (subunit 2)	0.417	0.355	−0.170	56.7	0.32

(63%) was employed as the solvent content parameter used in the solvent-flattening procedures.

Model Building. All the model building and correction procedures were carried out on a Silicon Graphics Indigo, using the program QUANTA version 4.0 (Molecular Simulations Inc.). Minimaps were used to locate the secondary structures in the 7α-HSDH molecule. At this stage, we became aware that the arrangement of most secondary structural elements in 7α-HSDH is similar to that in 3α,-20β-HSDH. The loop regions were traced with the aid of the program BONES as implemented in the program QUANTA. The quality of the MIR-SQ (defined above) electron density maps at 2.3 Å was so good that almost all the side chains could easily be identified. Furthermore, the nature of the heavy-atom binding sites (summarized in Table 3) ensured the validity of the chain tracing. Thus mercury peaks were found around the sulfur atoms of Cys13 and Cys65 in each subunit. Platinum peaks were found around the sulfur atoms of Met1 and Met156 in each subunit. In this way, the polypeptide chain segments corresponding to residues 1−193 and 210−251 for each subunit were built from the MIR-SQ electron density map at 2.3 Å resolution.

Structure Refinement. This was performed using the program X-PLOR version 3.1 (Brünger et al., 1987). Free *R* values (R_{free}) were used to monitor the refinement progress (Brünger, 1992). The initial protein atomic model built from the MIR-SQ electron density map was refined by simulated annealing procedures using the slow-cooling protocol (Brünger & Krukowski, 1990) against the 6.0−3.0 Å shell data. The *R*-factor for the 6.0−3.0 Å shell data dropped to 0.253 (R_{free} = 0.311) starting from the initial value of 0.440. In the initial stages, noncrystallographic symmetry restraints were imposed on the two subunits in an asymmetric unit. Temperature factors for all atoms were arbitrarily set to a constant value of 20 Å^2. To build a model for the exposed loop region (between the βF strand and the αG helix) where MIR-SQ electron density was rather weak, $2F_o - F_c$ and $F_o - F_c$ maps were calculated, and the model was interactively corrected and expanded with the program QUANTA. Data to 2.5 Å resolution were then included in the refinement. At this stage, the overall temperature factor and individual isotropic temperature factors were successively refined. The *R*-factor for 6.0−2.5 Å data dropped to 0.213 (R_{free} = 0.265). The resolution range used for the refinement was then expanded to 8.0−2.3 Å, and the noncrystallographic symmetry restraints were removed. After the second round of the refinement at a resolution range of 8.0−2.3 Å (R = 0.209, R_{free} = 0.287), peaks above 3.0σ in an $F_o - F_c$ map and having acceptable hydrogen-bonding geometry were considered to be bound water molecules. Water molecules having *B*-values greater than 60 Å^2 were excluded. The present model includes an NAD^+ molecule and all the nonhydrogen atoms except for the two C-terminal residues for each of the two subunits. In addition, 98 water molecules were included per asymmetric unit. The current *R*-factor is 0.182 (R_{free} is 0.265), for the resolution range of 8−2.3 Å ($F > 1.0\sigma_F$). The root-mean-square (rms)[1] deviations from idealities are 0.011 Å for bond lengths and 1.64° for bond angles. These statistics are summarized in Table 4. The stereochemistry of the model was verified using the software package PROCHECK (Laskowski et al., 1993). The secondary structures were assigned by the criteria of Kabsh and Sander (1983), as implemented in PROCHECK. The coordinate error was estimated from a Luzzati plot (Luzzati, 1952).

Model Building and Structure Refinement for the Ternary Complex. The model for the binary complex (excluding

Table 4: Refinement Statistics for the Binary Complex (or Holo Form) and the Ternary Complex of 7α-HSDH

	binary complex (laboratory data)[a]	ternary complex (laboratory data)[a]	ternary complex (synchrotron data)[a]
resolution range (Å)	8.0−2.3	8.0−2.3	8.0−1.8
no. of reflections ($F > 1.0\sigma_F$)	27230	27967	56376
completeness (%)	84.3	86.6	83.8
R-factor[b] (without low-resolution cutoff)	0.182 (0.264)	0.180 (0.256)	0.207 (0.252)
free *R*-factor[c] (without low-resolution cutoff)	0.265 (0.335)	0.250 (0.360)	0.253 (0.302)
no. of protein and NAD(H) atoms	3808[d]	3840[e]	3840[e]
missing residue/subunit	2	none	none
no. of product atoms	none	56[f]	56[f]
no. of water molecules	98	104	242
rms deviations from ideal values			
bond length (Å)	0.011	0.012	0.010
bond angles (deg)	1.64	1.58	1.67
Ramachandran plot statistics[g]			
% residues in most favored region	88.1	90.2	90.7
% residues in additional allowed region	11.5	9.3	8.8
% residues in generously allowed region	0.5	0.5	0.5

[a] See footnote *b* in Table 1. [b] *R*-factor = $\Sigma| |F_o| - k|F_c| |/\Sigma |F_o|$, where $|F_o|$ and $|F_c|$ are the observed and calculated structure factor amplitudes, respectively. [c] A subset of data (10%) was excluded from the target set for refinement and exclusively used for free *R* value calculation. [d] 1860 protein and 44 NAD^+ atoms per subunit. The two C-terminal residues (Leu254-Asn255) are not included. [e] 1876 protein and 44 NADH atoms per subunit. [f] 28 ligand atoms per subunit. The reaction product, 7-oxoglycochenodeoxycholic acid, was modeled as 7-oxolithocholic acid because the glycine moiety was missing in the electron density map. [g] As calculated by PROCHECK (Laskowski et al., 1993).

water molecules) as determined above was used as a starting model. Difference electron density maps clearly showed a group of electron densities corresponding to the steroid skeleton of the bound bile acid and indicated a large movement of the substrate-binding loop (a long loop located between the βF strand and the αG helix). Interactive model building and refinement cycles were carried out in a way similar to that described above. For all rounds of the refinement for the ternary complex, geometrical restraints were applied to the A−D rings of the steroid skeleton of bile acid according to the crystal structure of chenodeoxycholic acid (Lindley et al., 1980) except for position 7. Position 7 of the steroid skeleton of the product was modeled as being in the keto form (rather than the hydroxyl form). Water molecules having peaks above 3.0σ in an $F_o - F_c$ map and exhibiting acceptable hydrogen-bonding geometry were added to the model with the aid of the program X-Solvate as implemented in the program QUANTA version 4.1 (Molecular Simulations Inc.). The refinement statistics are summarized in Table 4.

RESULTS

Structure Determination and Quality Assessment. The structure of the binary complex of 7α-HSDH (or holo-7α-HSDH) was determined by the multiple isomorphous replacement method and refined to an *R*-factor of 0.182 at 2.3 Å resolution. The structure of the ternary complex of 7α-HSDH [complexed with NADH, 7-oxo-GCDCA (as reaction product), and possibly partially GCDCA (as substrate); see the section The Oxidation State of the Substrate for details] was determined by the difference Fourier method and refined to an *R*-factor of 0.207 at 1.8 Å resolution. Two representative ($|F_o| - |F_c|$) omit Fourier maps for the holoenzyme are shown in Figure 2. Two C-terminal residues in each subunit, which were not clearly visible, are not included in the current model for the holoenzyme. For the ternary complex, all residues in each subunit are included in the current model. On a Ramachandran plot (Ramachandran et al., 1963) for the current model of the holoenzyme, a total of 384 non-glycine and non-proline residues have their ϕ, ψ angles in the most favored (Morris et al., 1992) region of the Ramachandran plot, whereas the remaining 50 non-glycine and non-proline residues are in the additional allowed region. Only the two non-glycine residues, Thr145 and Arg216 in subunit 1, are in the generously allowed region. The corresponding two residues in subunit 2, having essentially the same conformation, barely fall in the additional allowed region. The reason for this slight anomaly is not clear because the electron densities for these two residues are clearly visible for both subunits 1 and 2 despite being in the loop region [but note the hydrogen bond system formed by the indole ring of Trp238 (described in the Intersubunit Contacts section) which might explain the anomaly related to Arg216]. The Ramachandran plot for the current model of the ternary complex appears similar to that for the holoenzyme. A plot of the average main-chain temperature factors (*B*-factor) is shown in Figure 3. The average *B*-factors for the holoenzyme are 32.2 and 27.8 Å^2 for the main-chain atoms of subunit 1 (thick and continuous) and subunit 2 (thin and continuous), respectively. The corresponding *B*-factors for the ternary complex are 31.3 and 27.7 Å^2 for the main-chain atoms of subunit 1 (thick and dashed) and subunit 2 (thin and dashed), respectively. The relatively high average values are due to exposed loop regions (between the βF strand and the αG helix) having very high temperature factors. We must admit that the model corresponding to the exposed loop region is of a rather biased nature. The difference in the *B*-factors between subunit 1 and subunit 2 (thick and thin lines respectively) is due to crystal packing. This difference is conspicuous in the N-terminal region (βA strand to αD helix, hereafter simply βA to αD). In subunit 1, this region is not in contact with the neighboring molecules. The *B*-factor difference between the binary and ternary complexes (continuous and dashed lines, respectively) is due to substrate binding (described later). This difference is most conspicuously seen in the substrate-binding loop (located between βF and αG). The coordinate errors estimated from Luzzati plots are between 0.25 and 0.30 Å for both the binary and ternary complexes.

Molecular Structure. Ribbon drawings of the 7α-HSDH tetramer are shown in Figure 4. This oligomeric structure appears to correspond to a natural state in solution (Yoshimoto et al., 1991). In the present crystal form two dimers are mutually related by the [110] crystallographic 2-fold rotation axis (or diad). The noncrystallographic diad in the asymmetric unit, which relates the two subunits in the dimer, is running perpendicular to this crystallographic diad. Thus the four subunits in a 7α-HSDH molecule are related by the 222 point group symmetry. Comparing the two subunits in an asymmetric unit, the rms difference is 0.32 Å for 253 pairs of α-carbons, which is only marginally larger than the estimated coordinate error (see above). The three mutually perpendicular diads in the dehydrogenase molecule are conventionally named *P*, *Q*, and *R* (Ghosh et al., 1991). In the present crystal, the *R*-axis coincides with the [110] crystallographic diad (see Figure 4a). As seen in Figure 4, the main body of the tetramer can be described as being oblate-shaped with the overall dimensions of 70 Å × 60 Å × 30 Å. Only the exposed loops located between the βF strand and the αG helix protrude from the main body. Each subunit of 7α-HSDH has an α/β doubly wound structure (Orengo et al., 1994) with a characteristic dinucleotide-binding motif called the Rossmann fold. As shown in Figure 5, the subunit of 7α-HSDH consists of a core β-sheet consisting of seven parallel β-strands sandwiched between the two arrays of three α-helices located on both sides of the β-sheet. In Figure 6, the folding topologies are schematically compared for 7α-HSDH, 3α,20β-HSDH, and dihydropteridine reductase (DHPR). As usual, each of the five βαβ motifs (such as the βA-αB-βB motif) appearing along the βA through the βF polypeptide chain segment exhibits a right-handed crossover. However, the last βαβ motif, βF-αG-βG, having a insertion of two short α-helices (αFG1 and αFG2) between βF and αG, exhibits a left-handed crossover. As seen in Figure 6, the overall folding topology of 7α-HSDH is almost completely identical with that of 3α,20β-HSDH. DHPR, on the other hand, exhibits a minor modification of the basic topology shared by 7α-HSDH and 3α,20β-HSDH: αC is missing while βH is added.

Intersubunit Contacts. The most extensive intersubunit interactions are made by the *Q*-axis-related subunits. The *Q*-axis interface comprises two αE and two αF helices (see Figures 4c and 7a). The αE and αF helices belonging to one subunit are respectively in contact with the αE and αF helices belonging to the other subunit (Figure 7a). In the

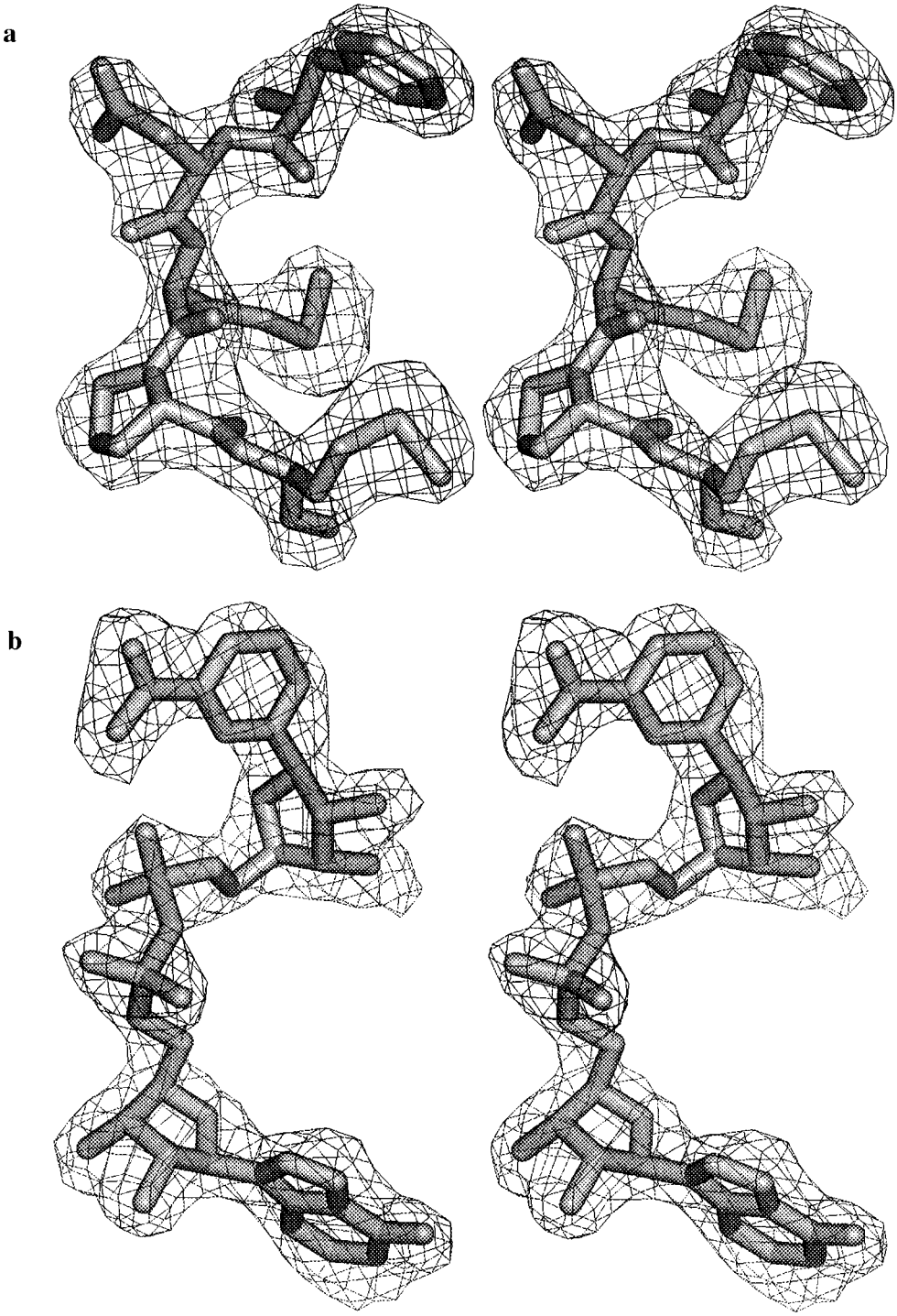

FIGURE 2: Representative portions of the omit (rather than $2|F_o| - |F_c|$) electron density maps calculated for the binary complex of 7α-HSDH (or holo-7α-HSDH) using the 8.0−2.3 Å resolution data for (a) residues 104−108 (Phe-Asp-Met-Pro-Met) in subunit 1 and (b) the NAD^+ molecule in subunit 1. The contour level is 3.0σ in both cases. These figures were produced with the program QUANTA (Molecular Simulations Inc.).

αE−αE interface (Figure 7b), large hydrophobic side chains (from Met108, Phe111, Tyr115, Val119, Phe120, and Phe123) face each other. A pair of salt bridges is formed between Arg112 and Glu116. Similar salt bridges are also found in 3α,20β-HSDH (Arg105−Glu109) (Ghosh et al., 1994a). In contrast, the αF−αF interface (Figure 7c) has no large hydrophobic side chains. Thus the two αF helices are closer to each other compared with the αE−αE interface. The αF−αF interface involves residues Thr157, Ala160, Ser161, Ala164, Ala165, His168, Leu169, and Asn172.

Interactions between the *P*-axis-related subunits are not so extensive. Similarly to the *Q*-axis interface, the *P*-axis interface can be described in terms of the αG−αG and βG−βG interfaces (Figure 7d). In the αG−αG interface, (1) the two benzene rings from the symmetry-related pair of Phe230 are stacked, (2) the side chain of Asn226 is hydrogen-bonded to the carbonyl oxygen of Ala235 from the other subunit, and (3) the extended amino terminus forms a hydrogen bond with the side chain of Gln222 from the other subunit and further undergoes electrostatic interaction with the side chain of Glu26 from the other subunit. In the loop region, (1) the indole ring of Trp238 forms hydrogen bonds with the carbonyl oxygens of Ile215 and Arg217 from the other subunit and (2) the indole ring of Trp238 appears to fill a

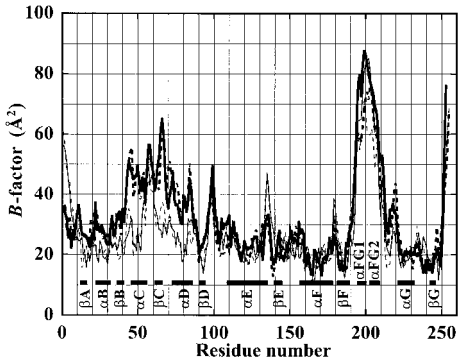

FIGURE 3: Plot of the mean main-chain temperature factors versus amino acid residue number for 7α-HSDH. Thick and thin lines, respectively, correspond to subunit 1 and subunit 2 in an asymmetric unit. Continuous and dashed lines, respectively, represent binary and ternary complexes. For both complexes, the corresponding laboratory data (see Table 4) were used. Synchrotron data for the ternary complex (see Table 4) were not used to avoid the effect of instrumental difference.

cavity in the other subunit and behave like a tenon. In the βF−βF interface, no direct interaction is found because the two antiparallel β-strands are too far away from each other for direct interaction.

In the present structure of 7α-HSDH, no direct interaction appears to be present in the *R*-axis interface. In contrast, in the case of 3α,20α-HSDH, the *R*-axis interface involves the interaction between the symmetry-related carboxyl-terminal residues.

The NAD⁺ Binding Site. As shown in Figure 2b, the electron density corresponding to the coenzyme NAD^+ is very well defined in the structure of the binary complex. The conformation of the NAD^+ ligand and its binding mode to the Rossmann fold are very similar to those found in 3α,-20β-HSDH (Ghosh et al., 1994a) and DHPR (Varughese et al., 1992). Thus the adenine and nicotinamide rings are oriented roughly perpendicular to the planes of the respective riboses resulting in an *anti* conformation for the adenine ring and a *syn* conformation for the nicotinamide ring. Both

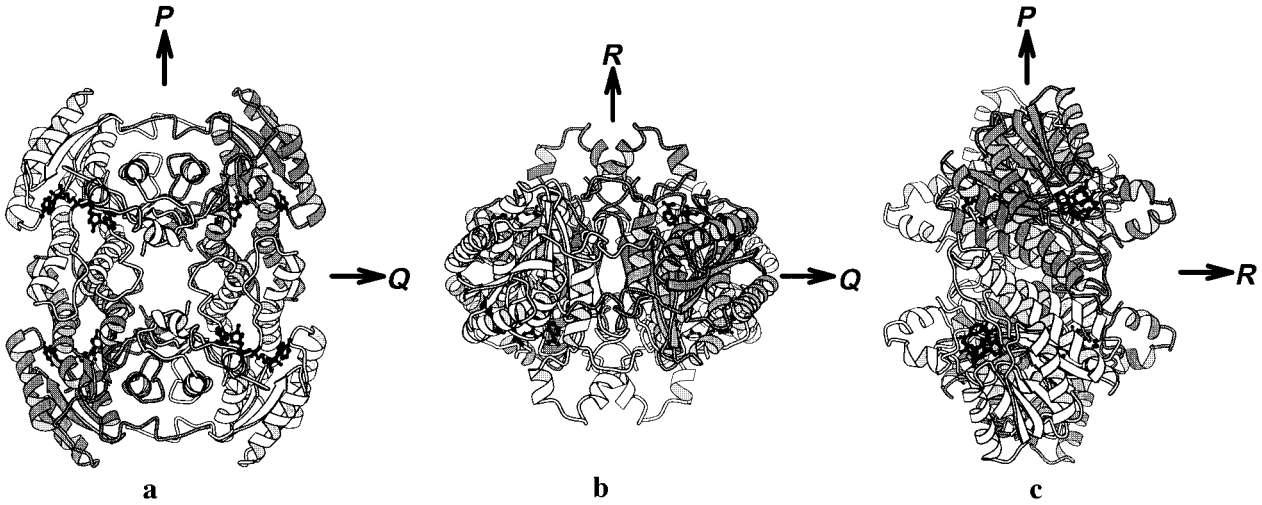

FIGURE 4: Ribbon representations of the tetramer of the binary complex of 7α-HSDH (or holo-7α-HSDH) viewed along each of the three noncrystallographic 2-fold axes. subunit 1 is darkened. Bound NAD^+ molecules are shown as ball-and-stick models. (a) View along the *R*-axis (coinciding with the [110] crystallographic 2-fold rotational axis) which is perpendicular to the plane of the paper. (b) View along the *P*-axis. (c) View along the *Q*-axis. These figures were produced with the program MOLSCRIPT (Kraulis, 1991).

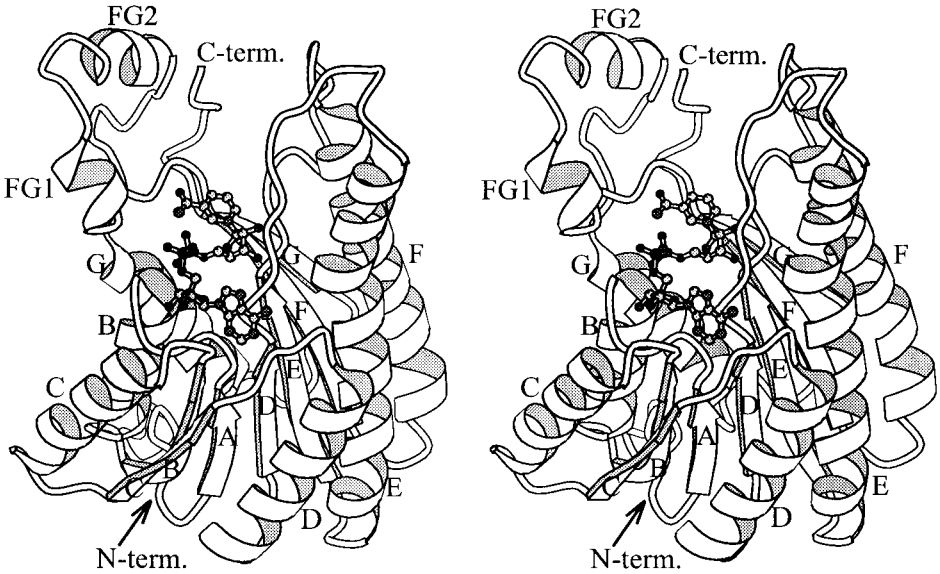

FIGURE 5: Stereoribbon drawing of the binary complex of the 7α-HSDH (or holo-7α-HSDH) monomer. The bound NAD^+ molecule is shown as a ball-and-stick model. Helices B through G and β-strands A through G, as well as the N- and C-termini, are marked. The upper depression is the active site cleft. The long loop containing the FG1 and FG2 helices (the substrate-binding loop) undergoes a large induced-fit movement upon binding to the substrate (see text). This figure was produced with the program MOLSCRIPT (Kraulis, 1991).

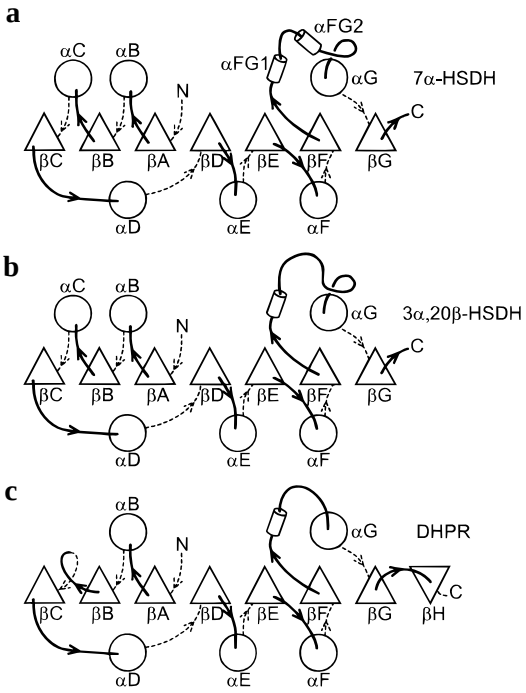

FIGURE 6: Comparison of the folding topologies found in the crystal structures of (a) 7α-HSDH, (b) 3α,20*β*-HSDH, and (c) DHPR. α-Helices are represented as circles and *β*-strands as triangles. Cylinders indicate short α-helices on the exposed loop (substrate-binding loop) region between the *β*F strand and the αG helix.

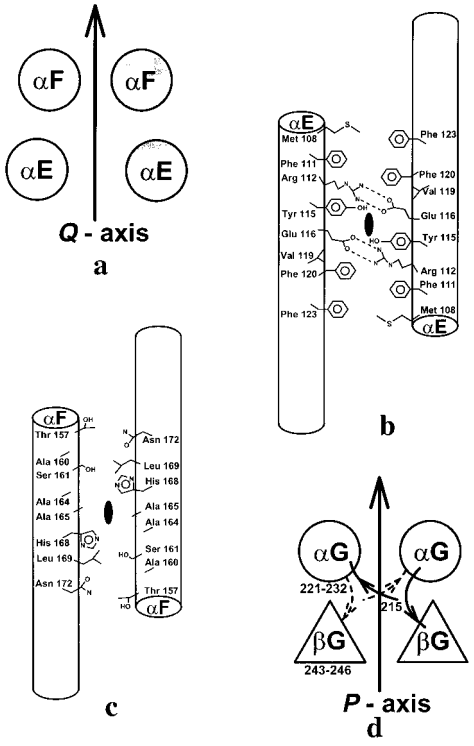

FIGURE 7: Schematic drawings of the subunit interfaces in the binary complex of 7α-HSDH (or holo-7α-HSDH). (a) The *Q*-axis interface. Shaded helices αE and αF belong to the same subunit and are parallel to each other. (b) The αE−αE interface viewed down the *Q*-axis (solid ellipsoid). Cylinders indicate α-helices. (c) The αF−αF interface viewed down the *Q*-axis (solid ellipsoid). (d) The *P*-axis interface. Shaded helix αG and strand *β*G belong to the same subunit and are parallel to each other.

ribose rings have ^{2}E (C2′-*endo*) puckering. The nomenclature for the coenzyme atoms and sugar puckering forms is adopted from the IUPAC−IUB nomenclature for polynucleotides (IUPAC−IUB Joint Commission on Biochemical Nomenclature, 1983). A parameter frequently used to express the degree of extension of the coenzyme molecule is the distance between C6 of adenine and C2 of nicotinamide in a *syn* conformation (Rossmann et al., 1975). This value is 14.4 Å for 7α-HSDH, which is very close to the value found in 3α,20*β*-HSDH (14.6 Å) or that found in DHPR (15.1 Å). Five hydrogen bonds exist between the NAD^+ ligand and the enzyme surface (Figure 8 and Table 5). The side chain of Asp42 is hydrogen-bonded to O2′A and O3′A of the adenosine ribose. The same hydrogen-bonding pattern involving an aspartic acid side chain and the adenosine ribose was also found in 3α,20*β*-HSDH and DHPR. The same kind of interaction involving an aspartic acid side chain and an adenosine ribose was found in the similar Rossmann folds in medium-chain dehydrogenases (Al-Karadaghi et al., 1994; Skarzynski et al., 1987; Piontek et al., 1990; Birktoft et al., 1989). The side chain of Lys163 forms hydrogen bonds with O2′N and O3′N of the nicotinamide ribose. The nicotinamide group resides deep in the putative active-site pocket and is connected to the enzyme surface through a hydrogen bond between the oxygen atom of the carboxamide and main-chain nitrogen of Ile192. The OG atom of Thr194 is located near the nitrogen atom of the carboxamide [OG1 (Thr194)···N7N (NAD): 4.2 Å]. Adenosine ribose and the pyrophosphate moiety are located on the Gly18-Gly24 turn located between *β*A−αB. As shown in Figure 9, this turn has a consensus sequence of Gly-X-X-X-Gly-X-Gly (X can be any amino acid; these three Gly residues are stressed in Figure 9). Unlike the case of medium-chain alcohol dehydrogenase (Al-Karadaghi et al., 1994), there is no direct interaction between the pyrophosphate bridge and any positively charged side chain of the enzyme. As shown in Figure 8, Asp68 in 7α-HSDH is located near the adenine ring of NAD^+ forming a rather poor (with respect to linearity) hydrogen bond [N6A (NAD)···OD2 (Asp68): 3.1 Å]. This aspartic acid residue had once been considered to be a conserved residue (Persson et al., 1991). However, Varughese et al. (1994) suggested that this aspartic acid residue would not be conserved in the SDR family, because it did not occupy geometrically equivalent positions between the cases of 3α,20*β*-HSDH and DHPR. In view of the present study, Asp68 in 7α-HSDH is geometrically equivalent to Asp60 in 3α,20*β*-HSDH but not Asp61 in DHPR.

Table 5: Possible Hydrogen Bonds between NAD^+ and 7α-HSDH in the Binary Complex (or Holo Form)

atom in NAD^+ atom in 7α-HSDH	distance (Å) subunit 1	distance (Å) subunit 2	mean distance (Å)
O2′A···OD2 (Asp42)	2.90	3.20	3.05
O3′A···OD1 (Asp42)	2.68	2.85	2.77
O2′N···NZ (Lys163)	2.86	2.77	2.82
O3′N···NZ (Lys163)	3.07	3.04	3.06
O7N···N (Ile192)	2.91	2.98	2.95

The Active Site of the Binary Complex of 7α-HSDH (or Holo-7α-HSDH). The putative active site is composed of the nicotinamide moiety of NAD^+, strictly conserved residues Tyr159 and Lys163 (stressed in Figure 9), and the C-terminal segment (see below). Tyr159 in 7α-HSDH corresponds to Tyr152 in *Drosophila* alcohol dehydrogenase (DADH),[1] another enzyme belonging to the SDR family (see Figure 9). The latter residue has been conceived as a catalytic residue (Chen et al., 1993). Lys163 in 7α-HSDH corre-

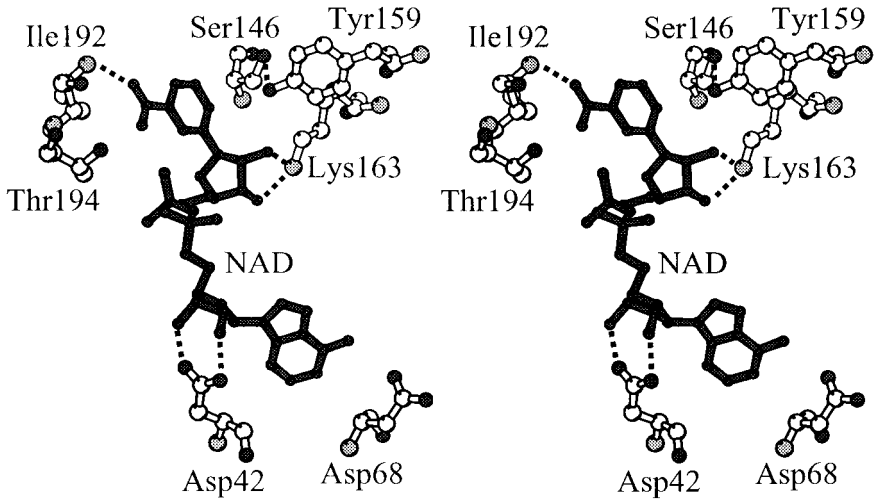

FIGURE 8: Mode of NAD^+ binding to the active site of the binary complex of 7α-HSDH (or holo-7α-HSDH). The bound NAD^+ molecule is shown in dark gray. Possible hydrogen bonds are indicated by dashed lines. This figure was produced with the program MOLSCRIPT (Kraulis, 1991).

```
                          <βA>       <---αB--->      <βB>          <---αC--->       <-βC>
                       10         20         30         40         50         60         70
7α-HSDH          MFNSDNLRLDGKCAIITGAGAGIGKEIAITFATA-GASVVVS*42*DINADAANHVVDEIQQLGGQAFACRCDIT
3α,20β-HSDH        NDLSGKTVIITGGARGLGAEAARQAVAA-GARVVLA*37*DVLDEEGAATARELG---DAARYQHLDVT
DHPR                 EARRVLVYGGRGALGSRCVQAFRAR-NWWVASI*37*DVVENEEA-----------SASVIV--K-
DADH               SFTLTNKNVIFVAG-LGGIGLDTSKELLKRDLKNLVIL*38*DRIENPAAIAELKAINKPVTVTFYPYDVT

                          <-----αD----->     <-βD->             <------------αE------------>
                                80         90        100         110        120        130
7α-HSDH          -------SEQELSALADFAISKLGKVDILVNNAGGGGPKPF--DMPMADFRRAYELNVFSFFHLSQLVAPEMEKNG
3α,20β-HSDH      -------IEEDWQRVVAYAREEFGSVDGLVNNAGISTGMFLE-TESVERFRKVVEINLTGVFIGMKTVIPAMKDAG
DHPR             MTDSFTEQADQVTAEVGKLLGD-QKVDAILCVAGGWAGGNAKSKSLFKNCDLMWKQSIWTSTISSHLATKHLKE--
DADH             -------VPIAETTKLLKTIFAQLKTVDVLINGAGILDDHQIERT--IAVNYTGLVNTTTA---ILDFWDKRKGGP

                   <--βE->               <-------------αF------------->   <--βF-->
                  140            150            160        170        180        190
7α-HSDH          GGVILTIT*146*SMAAENKNINMTS*159*YASSKAAASHLVRNMAF--DLGEKNIRVNGIAPGAIL*194*T
3α,20β-HSDH      GGSIVNIS*139*SAAGLMGLALTSS*152*YGASKWGVRGLSKLAAV--ELGTDRIRVNSVHPGMTY*187*T
DHPR             GGLLTLAG*133*AKAALDGTPGMIG*146*YGMAKGAVHQLCQSLAGKNSGMPSGAAAIAVLPVTLD*183*T
DADH             GGIICNIG*139*SVTGFNAIYQVPV*152*YSGTKAAVVNFTSSLAK--LAPITGVTAYTVNPGITR*187*T

                   <αFG1>   <-αFG2->              <----αG---->          <βG>                 <-βH->
                     200        210            220        230        240        250
7α-HSDH          DALKSVIT-PEIEQKMLQHT-----PIRRLGQPQDIANAALFLCSPAASWVSGQILTVSGGGVQELN
3α,20β-HSDH      PMTAETGIRQGEGN--YPNT-----PMGRVGEPGEIAGAVVKLLSDTSSYVTGAELAVDGGWTTGPTVKYVMGQ
DHPR             PMNRKSMPEADFS---------------SWTPLEFLVETFHDWITGNKRPNSGSLIQVVTT-------------DGKTELTPAYF
DADH             TLVLVHTFNSWLDVEPQVAEKLLAHPTQPSLACAENFVKAIELNQNGAIWKLDLGTLEAIQWTKHWDSGI
```

FIGURE 9: Alignment of the amino acid sequences of some enzymes belonging to the short-chain dehydrogenase/reductase family which are most relevant to descriptions given in the text. The residue numbers are for 7α-HSDH. A more exhaustive table can be found in Jörnvall et al. (1995). Amino acid residues belonging to the secondary structural elements (shown on top) are underlined. Highly conserved residues are stressed and, for some residues, preceded by respective residue numbers. The abbreviations used are as follows: 7α-HSDH, 7α-hydroxysteroid dehydrogenase from *E. coli*; 3α,20*β*-HSDH, 3α,20*β*-hydroxysteroid dehydrogenase from *Streptomyces hydrogenans*; DHPR, rat liver dihydropteridine reductase; DADH, *Drosophila* alcohol dehydrogenase. Except for DADH, the alignment is based on available three-dimensional structures of 7α-HSDH (present study), 3α,20*β*-HSDH (Ghosh et al., 1994a), and DHPR (Varughese et al., 1992).

sponds to Lys156 in DADH. The latter residue has been regarded as lowering the pK_a value of Tyr152 in DADH (Chen et al., 1993). The distance between OH (Tyr159) and NZ (Lys163) is 5.1 Å. The ϵ-amino group of Lys163 forms a bifurcated hydrogen bond to both the O2′N and O3′N atoms of the nicotinamide ribose [O2′N (NAD)···NZ (Lys163), 2.8 Å; O3′N (NAD)···NZ (Lys163): 3.1 Å]. The residue Ser146 is located near Tyr159, giving rise to a hydrogen bond [OG (Ser146)···OH (Tyr159): 2.9 Å]. The "B-face" of the nicotinamide ring points toward the putative active site cleft. The peptide nitrogen of Ile192 forms a hydrogen bond with the carboxamide oxygen of the nicotinamide ring [N (Ile192)···O7N (NAD): 3.0 Å]. Thr194 is located near the carboxamide nitrogen of the nicotinamide ring [OG (Thr194)···N7N (NAD): 4.2 Å]. As seen in Figure 5, the third component of the putative active site is the C-terminal

segment (residues 250−253) belonging to the same subunit (two C-terminal residues are missing in the binary complex). Thus the active site of 7α-HSDH is completed within one subunit. In contrast, in the case of 3α,20*β*-HSDH, the C-terminal segment as the third component is contributed from the other *R*-axis-related subunit.

Conformation Change upon Substrate Binding. As shown in Figure 10a, a large-scale conformation change occurs upon substrate binding, that is, upon transition from the binary (complexed with NAD^+) to the ternary [complexed with NADH, 7-oxo-GCDCA (as reaction product), and possibly partially GCDCA (as substrate)] complexes of 7α-HSDH. These conformation changes occur in the substrate-binding loop (between the *β*F strand and the αG helix: residues 195−210) and the C-terminal segment (residues 250−255). The largest change in Cα position (*ca.* 8.5 Å) is observed for Val200. Comparing the substrate-binding loops in the two states, we find that the conformations of the major portion of the substrate-binding loop (residues 195−210) are almost unchanged. Thus the large structural change is mainly due to a swinging of the loop as a whole with the main-chain connections at Thr194 and Gln211 acting as the hinges.

The Substrate Binding Mode. Below we will show the first evidence among the enzymes of the SDR family that the conserved tyrosine (Tyr159 in 7α-HSDH) and serine (Ser146 in 7α-HSDH) residues most probably directly interact with the susceptible oxygen atom (the 7-oxo group, indicated by a character "7" in Figure 10b) of the substrate, although the observation cannot be conclusive since the molecular species present in the ternary complex has not yet been fully characterized (see the section The Oxidation State of the Substrate below). As shown in Figure 10a, the product molecule (colored yellow), as an apparently dominant species (see the section The Oxidation State of the Substrate below), occupies the active-site cleft surrounded by the substrate-binding loop and the C-terminal segment (both colored red). As seen in Figure 10b, the electron density corresponding to the A−D rings of the steroid skeleton of the product is very well defined despite the fact that this is an omit difference (rather than $2|F_o| - |F_c|$) Fourier map. The most probably dominant product molecule, 7-oxoglycochenodeoxycholic acid, was modeled as 7-oxolithocholic acid, because the electron density corresponding to the glycine moiety (conjugated to GCDCA at position 24; see Figure 1) was missing. Although the electron density for the tail part (see Figure 10b) of the product was poor, the orientation of the steroid skeleton was easily determined because the *cis* junction between the A and B rings of the steroid skeleton was clearly discernible from the electron densities. There are two types of interaction between the product and the enzyme. One is the hydrophobic interactions between the side chains of Pro101, Val200, and Leu254 and the B−D rings of the steroid skeleton of bile acid. The other is the hydrogen bond between Asn151 and the hydroxyl group at position 3 of the steroid skeleton of the bile acid [ND (Asn151)···O3 (product): 3.0 Å].

The residues that can directly interact with the oxygen atom at position 7 of the steroid skeleton of bile acid are Tyr159 [OH (Tyr159)···O7 (product): 2.8 Å] and Ser146 [OG (Ser146)···O7 (product): 2.6 Å]. In the binary complex, Ser146 is hydrogen-bonded to Tyr159 [OG (Ser146)···OH (Tyr159): 2.9 Å]. In the ternary complex, however, this hydrogen bond is almost broken [OG (Ser146)···OH (Tyr159): 3.7 Å], and a stronger hydrogen bond is formed between the side chain of Ser146 and the susceptible oxygen atom of the product molecule [OG (Ser146)···O7 (product): 2.6 Å]. Surprisingly, in the case of the 3α,20*β*-HSDH−carbenoxolone (as an inhibitor) *binary* (without NADH) complex (Ghosh et al., 1994b), the opposite effect occurs upon inhibitor binding: the distance OG (Ser139)···OH(Tyr152), which is 3.8 Å in the NADH complex, becomes *shorter* (2.8 Å) in the inhibitor complex. This opposite effect may be related to the fact that the ternary complex in the present study presumably represents at least some features of a true *productive* binding mode while the inhibitor complex of 3α,20*β*-HSDH devoid of NADH does not (see Discussion).

The Oxidation State of the Cofactor. To determine the oxidation state of the nicotinamide moiety of the cofactor in the crystals, the absorbance at 340 nm was measured, before X-ray data collection, for the solutions in which binary complex crystals were soaked, using the method as described by Harrison et al. (1994). First, a few pieces of the binary complex crystals (before X-ray data collection) were soaked at 20 °C in 0.4 mL of a freshly prepared standard solution containing buffer, precipitant, and 2.8 mM NAD^+ (see Materials and Methods) for 12 h. The resultant solution did not show significant absorbance at 340 nm, indicating that at least the major portion of the cofactor in the binary complex remained as NAD^+ (rather than NADH). Second, a separate few pieces of the binary complex crystals (before X-ray data collection) was soaked at 20 °C in 0.4 mL of a freshly prepared substrate solution containing buffer, precipitant, 2.8 mM NAD^+, and 5 mM substrate (GCDCA) (see Materials and Methods) for 2 days. This solution showed significant absorbance at 340 nm, indicating that the relevant reaction occurred in these crystals resulting in the conversion of the significant proportions of the substrate (GCDCA) and NAD^+ into the product (7-oxo-GCDCA) and NADH, respectively. The concentration of NADH in this resultant solution was estimated to be 2.25 mM (the molecular extinction coefficient for NADH at 340 nm was assumed to be 6220) and that of the remaining NAD^+ was estimated to be 0.55 mM. On the other hand, in a separate experiment, the dissociation constant (K_d value) for NADH (93 *μ*M) was found to be lower than that for NAD^+ (221 *μ*M) (Yoshimoto et al., unpublished results). These observations taken together, it will be justified to assume that the major cofactor species existing in the present ternary complex crystals must be NADH rather than NAD^+.

For obtaining a direct proof of this argument, a large number of the ternary complex crystals as prepared above (after washing with PEG 6000 solution without the cofactor) were dissolved in a mere buffer solution (pH 8.5 buffered by 100 mM Tris). This solution showed significant absorbance at 340 nm, indicating that NADH was in fact present in the ternary complex crystals. It was calculated that, in this solution, the total amount of NADH corresponds to *ca.* 80% of that of the protein on a molar basis.

These two observations taken together, we would conclude that, most probably, NADH must be the major cofactor species in the present ternary complex crystals.

From a crystallographic point of view, we have noticed an apparent difference in the planarity of the carboxamide group with its attached (pyridine) ring between the case of the binary (NAD^+) complex and that of the ternary (at least

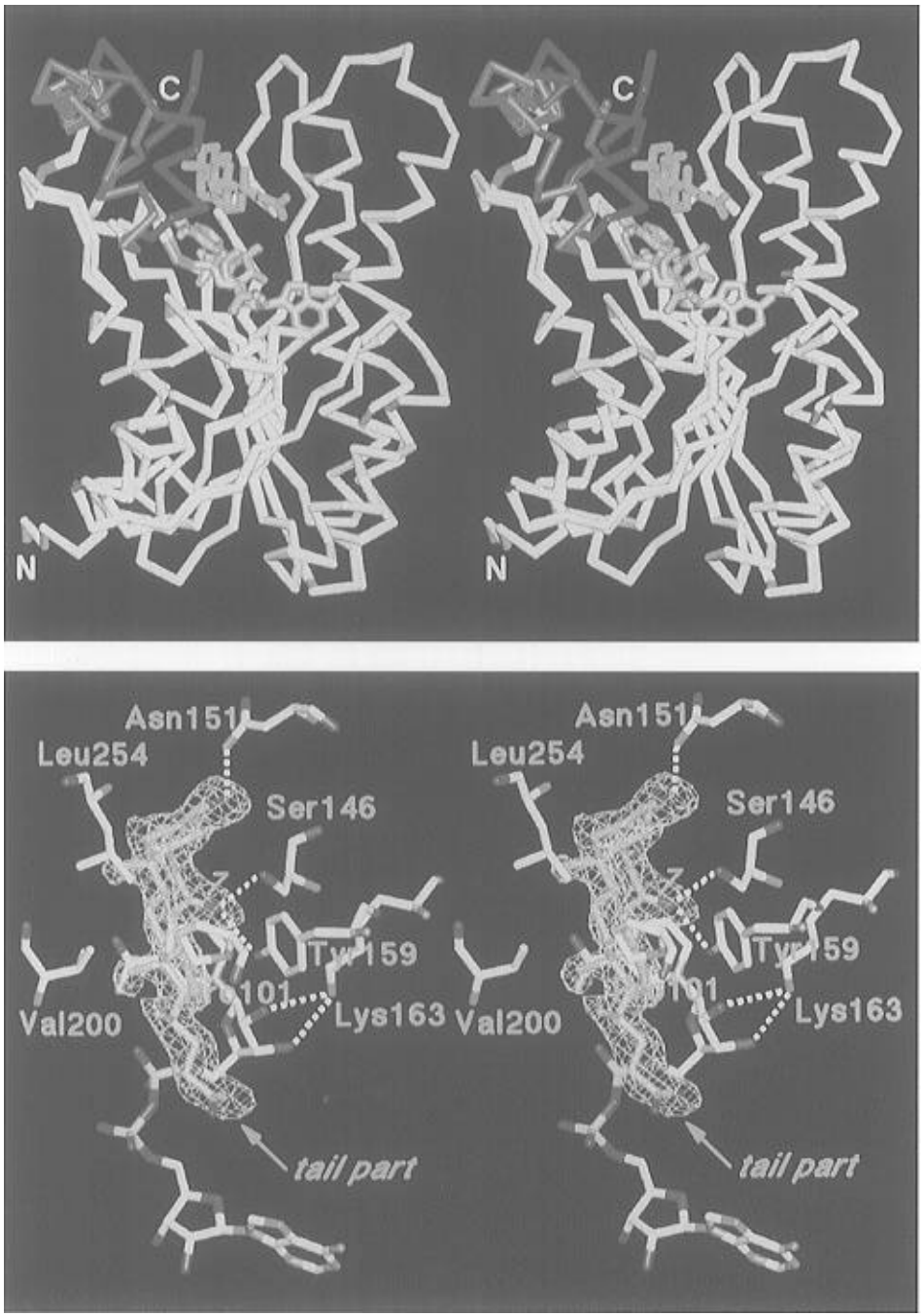

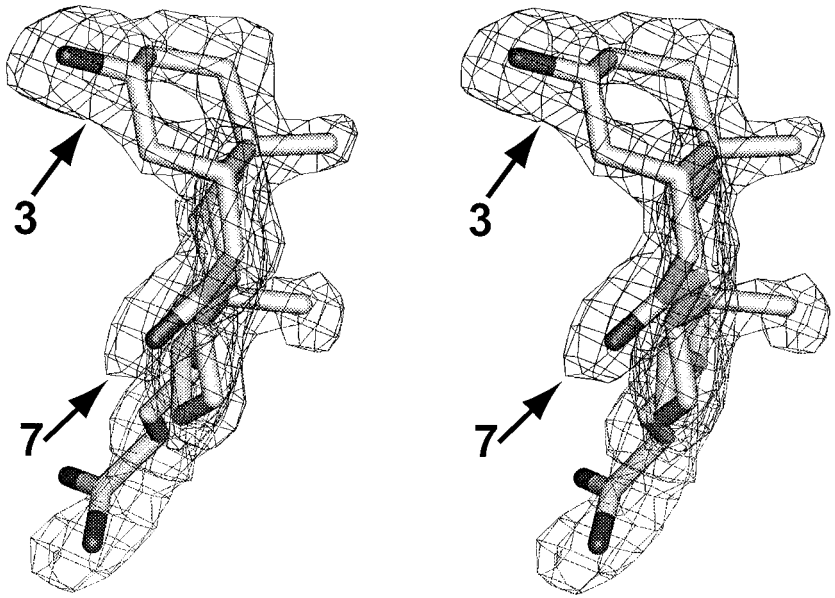

FIGURE 10: Binding mode of NAD(H) and a reaction product, 7-oxo-GCDCA (possibly partially mixed with a substrate, GCDCA), as shown on the overall polypeptide skeleton of 7α-HSDH. (a, top left) Stereo diagram showing the superimposition of the binary (complexed with NAD^+) and ternary [complexed with NADH and the reaction product (substrate)] complexes of 7α-HSDH. The core part of the Cα chains, which is almost identical between the two complexes, is colored white, while the segments with different conformation (residues 195−210 and 250−255) are colored green for the binary complex and red for the ternary complex. The similarly bound NAD(H) molecules are colored pink. The reaction product (modeled as 7-oxolithocholic acid, see text; possibly partially mixed with the substrate GCDCA) is colored yellow. The top central cavity accommodating the NAD(H) molecule and the reaction product (substrate) is the active site cleft (see text). Highly conserved proline residues (Pro189 and Pro214) referred to in the text are colored blue. (b, bottom left) Stereo diagram showing the active site cleft in the ternary complex of 7α-HSDH. Protein and NADH atoms are colored white (carbon), red (oxygen), blue (nitrogen), or yellow (phosphorus). Catalytic residues (Tyr159, Ser146, and Lys163) and substrate-binding residues (Pro101, Val200, Leu254, and Asn151) are shown. Possible hydrogen bonds are indicated by dashed lines. The reaction product molecule (colored pink) (possibly partially mixed with the substrate) is superimposed on the ($|F_o| - |F_c|$) omit electron density (using the 8.0−1.8 Å resolution shell data) contoured at 3.0σ. To exclude a bias toward any type of conceived model, the structure was specifically refined in the absence of the product molecule before the map calculation (see the section The Oxidation State of the Substrate). For the reaction product, the site of attachment of the tail part referred to in the section The Substrate Binding Mode is indicated. Also the position of the susceptible 7-oxo group is indicated by the character 7. (c, top right) Stereo diagram showing the reaction product in the active site of the ternary complex of 7α-HSDH. The final refined model of the reaction product molecule (colored light gray for carbon and dark gray for oxygen) is superimposed on the omit electron density map (using the 8.0−1.8 Å resolution shell data) calculated in the same way as in (b). This omit map is not biased toward any type of conceived molecular species (see the section The Oxidation State of the Substrate for details). Note that position 7 of the steroid skeleton appears flat. These figures were produced with the program QUANTA (Molecular Simulations Inc.).

largely NADH) complex. The planarity can be discussed by using the θ angle defined as a torsion angle around the C2N−C3N−C7N−O7N bond (IUPAC−IUB Joint Commission on Biochemical Nomenclature, 1983) where the last letter N stands for the nicotinamide moiety. The structures of both the binary and ternary complexes have been refined using the same refinement parameter for the cofactor (default parameter file, "param.nad", provided in X-PLOR). The final θ angle turned out to be 163° for NADH in the ternary complex, apparently indicating a significant deviation from the carboxamide−pyridine ring planarity. The value for the binary (NAD^+) complex turned out to be 175°, apparently indicating no significant deviation from planarity. Here we must note, however, that OG of Thr194 is located much closer to N7N of the cofactor (3.0 Å) in the ternary complex. The corresponding distance is 4.2 Å in the binary (NAD^+) complex (see Figure 8 showing the NAD^+ binding in the binary complex where OG and N7N are thus not connected). This remarkable difference in the hydrogen bond scheme may well affect the θ values and thus the planarity. Thus we believe it safer to avoid discussion about the oxidation state of the nicotinamide group based on the carboxamide−pyridine ring planarity alone.

The Oxidation State of the Substrate. To determine the molecular species present in the ternary complex crystal, it is desirable to know the binding constants of the substrate (reduced substrate) and the product (oxidized substrate) in the presence of the cofactor. Unfortunately, we were not able to do such an experiment since only a minute amount of the product 7-oxo-GCDCA was available to us.

In the hope of crystallographically clarifying the nature of the substrate/product species in the active site, we have finally collected 1.8 Å (compared with 2.3 Å for the previous laboratory data) resolution synchrotron data (see the section X-Ray Data Collection and Processing in Materials and Methods) for the ternary complex. We then refined the structure against the synchrotron data without incorporating the substrate/product portion. The amplitude (F_c) and the phase angle calculated from such a partial structure were then used to calculate an $F_o - F_c$ difference Fourier (or omit) map, which is unbiased toward any form of the substrate/product species. In this omit map (Figure 10c), position 7 of the steroid skeleton appears flat, indicating that the product (having an sp^2 carbon at position 7), rather than the substrate (having an sp^3 carbon at position 7), represents the molecular species of the largest fraction. Apparently in accord with this observation, the present crystal was prepared at pH 8.5, an optimum pH for oxidation by 7α-HSDH but an unfavorable pH for reduction (see the section Preparation of the Ternary Complex Crystals). The above observation tends to indicate that the enzyme−NADH−product (7-oxo−GCDCA) complex represents the molecular species of the largest fraction present in the ternary complex crystal.

More rigorously, however, it would be unnatural to assume that there remains no unconverted substrate molecule at all in the active site of the present ternary complex since approximately 1.8 times molar excess of the substrate existed in the substrate solution used for preparing the ternary complex (see the above section The Oxidation State of the Cofactor). However, all the spectroscopic evidence and new crystallographic evidence as described above taken together, it will be justified to argue that the molecular species of the *largest fraction* in the active site must be the product (rather than substrate) complex. Hereafter, when rigorousness is required, we will describe the present ternary complex as the enzyme complexed with NADH, product, and possibly partially with substrate.

DISCUSSION

Molecular Recognition of the Conjugated and Unconjugated Substrates by 7α-HSDH. As shown in Figure 10b, the electron density for the tail part (a conjugated glycine residue attached at position 24; see Figure 1) of the product molecule, 7-oxo-GCDCA, is poor, while that for the steroid skeleton of the product molecule (up to position 24; see Figure 1) is very well defined. This fact shows that the conjugated glycine part of the substrate is not tightly bound to the enzyme surface. Therefore, we speculate that the binding strength of the bile acid compounds having the same steroid skeleton as 7α-HSDH would be almost independent of the presence of the conjugated part or the nature of the conjugated part. A series of K_m values recently determined by Yoshimoto et al. (unpublished experiments) for several conjugated and unconjugated substrates appear to support the above notion. Thus the K_m values for glycochenodeoxycholic acid (glycine-conjugated form of chenodeoxycholic acid), taurochenodeoxycholic acid (taurine-conjugated form of chenodeoxycholic acid), and chenodeoxycholic acid have been determined to be not significantly different: they are 68, 61, and 72 μM, respectively.

The Catalytic Residues. Here we will focus on the conserved residues located around the putative active site. Among the enzymes belonging to the SDR family, a consensus sequence Tyr-X-X-X-Lys [X can be variable; see Figure 9 where the Tyr (159 in 7α-HSDH) and Lys (163 in 7α-HSDH) residues are stressed] is conserved in the putative active site (Persson et al., 1991). As seen in Figure 10b, these two residues are in fact located around the substrate analogue in the ternary complex of 7α-HSDH. Some mutagenesis studies have been done for these conserved tyrosine and lysine residues (Ensor & Tai, 1991; Albalat et al., 1992; Obeid & White, 1992; Chen et al., 1993; Cols et al., 1993; Whitely et al., 1993). All of these mutagenesis studies clearly show that the conserved tyrosine residue is essential for catalysis (for the role of the conserved lysine, see next section). In accord with this notion, the Tyr159Phe mutant of 7α-HSDH completely lost the enzymatic activity (Yoshimoto et al., unpublished experiments).

Apart from Tyr159, Ser146 in 7α-HSDH is also located near the substrate analogue (Figure 10b). This residue is almost conserved among the enzymes of the SDR family, but there have been no mutagenesis studies for this serine residue. Ser146 in 7α-HSDH is geometrically identical to Ser139 in 3α,20β-HSDH, but it is replaced by alanine in DHPR. The present study indicates that Tyr159 and Ser146 in 7α-HSDH most probably directly interact with the oxygen atom at position 7 of the steroid skeleton of the bile acid in the *productive* binding mode. Similar observation that the conserved tyrosine residue directly interacts with an inhibitor has been made for the case of the 3α,20β-HSDH−inhibitor complex (Ghosh et al., 1994b) although this complex was a rather unnatural binary complex (an enzyme−inhibitor complex in the absence of NADH).

The Role of the Conserved Lysine Residue. As seen in Figure 9, Lys163 in 7α-HSDH (or Lys150 in DHPR, Lys156

in DADH, and so on, these residues are stressed) is strictly conserved. Chen et al. (1993) showed that the Lys156Arg mutant of DADH exhibits a similar K_m value for NAD^+ as in the wild-type enzyme, while it exhibits higher K_m values than in wild-type enzyme for alcohol substrates. Their explanation for these results, in the absence of relevant crystal structure, is that Lys156 in DADH must be involved in the interaction of the substrate (rather than the cofactor) with the enzyme. Varughese et al. (1994), however, showed crystallographically that Lys150 in DHPR donates a hydrogen bond to the 2′-hydroxyl group of the nicotinamide ribose of NADH. Similarly, Lys163 in 7α-HSDH was found to form a hydrogen bond to the 2′- and 3′-hydroxyl groups of the nicotinamide ribose of NAD(H) in both binary and ternary complexes (Figure 8). A similar binding mode was also found in the enzyme−inhibitor complex of 3α,20β-HSDH (Ghosh et al., 1994b). Thus we would interpret the change in K_m value for alcohol substrates observed in the Lys156Arg mutant of DADH (Chen et al., 1993) as being due to indirect influences on the active site caused by the different environment of the nicotinamide ribose of NAD^+. Furthermore, Chen et al. (1993) proposed that Lys156 in DADH lowers the pK_a value of tyrosine to facilitate catalysis at neutral pH. The optimum pH of 7α-HSDH is pH 8.5 (Yoshimoto et al., 1991). Usually, the phenolic group of the tyrosine side chain has a pK_a value of about 10. If Tyr159 is deprotonated in the initial stage of the catalysis as proposed by Chen et al. (1993), its pK_a value must be lowered through the effect of the local environment. Lys163 in 7α-HSDH is likely to perform this role, considering the proximity of its ϵ-amino group [NZ (Lys163)···OH (Tyr159): 4.3 Å in the ternary complex]. Indeed, Yoshimoto et al. (unpublished experiments) deduced the presence of an amino acid residue having a pK_a value of 7.7 from enzyme kinetic analysis. In conclusion, Lys163 in 7α-HSDH has two critical roles: the interaction with the 2′- and 3′-hydroxyl groups of the nicotinamide ribose (cofactor binding) and the lowering of the pK_a value of the hydroxyl group of Tyr159.

Other Residues in the Active Site. As shown in Figure 8, the peptide nitrogen of Ile192 forms a hydrogen bond with the carboxamide oxygen of the nicotinamide ring in 7α-HSDH. Apparently because the main-chain (rather than side-chain) atom is the hydrogen bond donor, this residue is not conserved: Thr185 in 3α,20β-HSDH and Leu181 in DHPR. Examining Figure 8, one sees that the hydroxyl group of Thr194 in 7α-HSDH has the potential to interact with the carboxamide nitrogen of the nicotinamide ring although the OG (Thr194)···N7N (NAD) distance is rather long, 4.2 Å, in the present refined structure. This distance becomes shorter [OG (Thr194)···N7N (NAD): 3.0 Å] in the ternary complex owing to its hinge motion (described later). This threonine residue corresponds to Thr187 in 3α,20β-HSDH or Thr183 in DHPR. These three threonine residues appear to occupy geometrically equivalent positions.

In summary, we propose the roles of the residues located in the active site of 7α-HSDH as follows: Tyr159 plays an essential role as a basic catalyst; Ser146 may play an important role in catalysis; Lys163 is important in cofactor binding and in lowering the pK_a value of Tyr159; the side-chain hydroxyl of Thr194 and the main-chain amide group of the residue two residues upstream from Thr194 are important in properly orienting the nicotinamide ring. With the aim of clarifying the roles of these residues, enzyme kinetics and crystallographic studies are in progress in T. Yoshimoto's laboratory for various modified 7α-HSDH's produced by site-directed mutagenesis techniques.

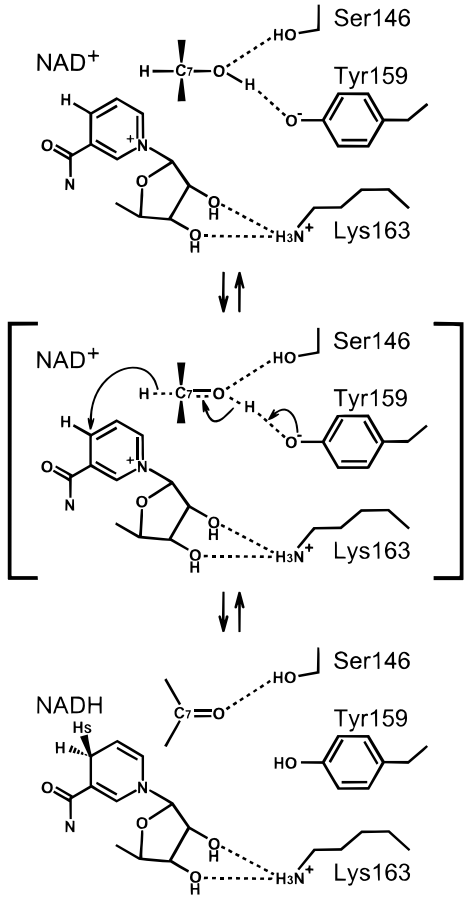

FIGURE 11: Proposed catalytic mechanism for 7α-HSDH taking the new structural features found in the present crystal structure analyses into consideration (see text). The susceptible part of the substrate, the Ser-Tyr-Lys triad (see text), and the nicotinamide nucleoside moiety of NAD^+ (or NADH) are shown.

Proposed Catalytic Mechanism Based on the Present Crystal Structure. The present crystal structure of the ternary complex of 7α-HSDH [complexed with NADH, 7-oxo-GCDCA (as a reaction product), and possibly partially GCDCA (as a substrate)] must be representing at least some features of a truly *productive* binding mode. The following arguments about the reaction product, however, should be taken as essentially speculative since the nature of the molecular species present in the ternary complex has not yet been fully characterized. The reaction product is most probably bound (1) with its α-face oriented toward Tyr159 such that the C7-O group resembles a 7α-hydroxyl group of the substrate and (2) with its β-face oriented toward the B-face of the nicotinamide ring of NAD(H) such that the β-hydride ion can be directly transferred to position 4 of the B-face of the nicotinamide ring. On the basis of this observation and other observations summarized in the above section taken together, we propose a catalytic mechanism for 7α-HSDH as follows (Figure 11).

In the first step (Figure 11a), the deprotonated phenolic group of Tyr159 forms a hydrogen bond with the hydroxyl group attached to position 7 of the steroid skeleton of the substrate. The hydroxyl group of Ser146 may also form a hydrogen bond with the substrate, stabilizing its position. In the second step (Figure 11b), the deprotonated tyrosine

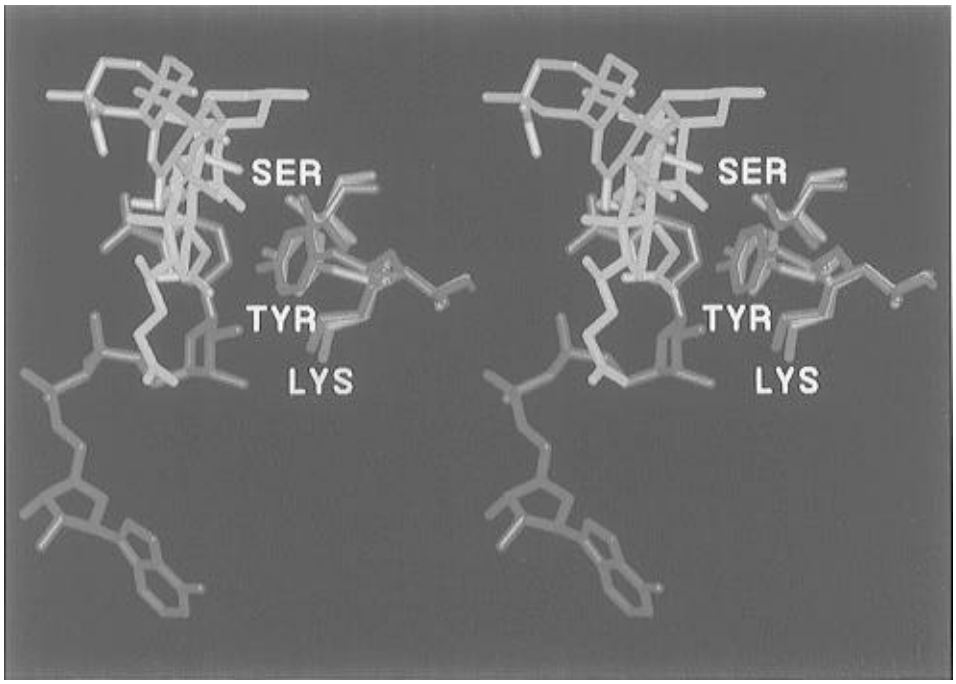

FIGURE 12: Stereo diagram showing the distinct binding modes of the substrate analogues relative to the Ser-Tyr-Lys triad and bound NADH molecule. The (Ser146, Tyr159, Lys163) triad in 7α-HSDH and the (Ser139, Tyr152, Lys156) triad in 3α,20β-HSDH are respectively colored red and green. The almost equivalently disposed NADH molecules (colored red) are represented by the molecule found in 7α-HSDH. As for the substrate analogues, the reaction product, 7-oxo-GCDCA, found in the *ternary (with NADH)* complex of 7α-HSDH is colored yellow, while the competitive inhibitor, carbenoxolone, found in the *binary (without NADH)* complex of 3α,20β-HSDH is colored blue. The least-squares fitting was done with respect to 35 pairs of α-carbon atoms belonging to the seven-stranded parallel β-sheet (βA to βG). The rms deviation for these α-carbon atoms was 0.55 Å. This figure was produced with the program QUANTA (Molecular Simulations Inc.).

residue acts as a catalytic base to extract a hydrogen from the hydroxyl group of the substrate. Concomitantly, NAD^+ accepts a hydrogen liberated from position 7 of the steroid skeleton onto the B-face of the nicotinamide ring at position 4. The reaction intermediate would be stabilized by a hydrogen bond to the hydroxyl group of Ser146. Because Tyr159 acts as a catalytic base, it must be deprotonated from the outset and this must occur at the optimum pH (8.5) of the enzyme 7α-HSDH. As mentioned above, the unusually low pK_a value of the tyrosyl residue may well be realized through the presence of the charged side chain of Lys163 (see Figure 11). It should be recalled here that the same side chain of Lys163 plays another role as a stabilizer of the position of the nicotinamide moiety of NAD(H) through a bifurcated hydrogen bond to both the 2′- and 3′-hydroxyl groups of the ribose moiety of the nicotinamide nucleotide (see Figure 8). The mechanism proposed here is basically similar to that proposed by Chen et al. (1993) in that the conserved tyrosine (Tyr159) acts as a catalytic base. However, a new feature, that a serine residue (Ser146) stabilizes the reaction intermediate, has been incorporated on the basis of the crystal structure elucidated in the present study. Moreover, the role of the conserved lysine residue (Lys163) has been considerably modified (as described above) compared with that inferred in Figure 5 of Jörnvall et al. (1995), where the presence of a direct hydrogen bond between the side chain of Lys156 (in 3α,20β-HSDH) and that of Tyr152 (in 3α,20β-HSDH) was postulated.

The Ser-Tyr-Lys Triad and the Binding Orientations of the Steroid Skeleton. Comparing the geometry of the substrate-(inhibitor-) binding site in the ternary complex of 7α-HSDH with that of the enzyme−inhibitor complex of 3α,20β-HSDH (Ghosh et al., 1994b), we note that the three-dimensional disposition of the Ser-Tyr-Lys triad is extremely well conserved (Figure 12). The triad is a set of Tyr159, Ser146, and Lys163 in the case of 7α-HSDH and a set of Tyr152, Ser139, and Lys156 in the case of 3α,20β-HSDH. This geometrical conservation strongly indicates that the two enzymes share a common catalytic mechanism in which the triad must be playing a central role. We also note the difference in binding orientations of the steroid skeleton in the active site: the bile acid in the active site of 7α-HSDH and the bound licorice-derived steroidal inhibitor in the active site of 3α,20β-HSDH are oriented roughly perpendicular to each other (see Figure 12). Of course, this difference is due to the fact that 7α-HSDH attacks the medium portion of the steroid skeleton while 3α,20β-HSDH attacks the two peripheral portions of the steroid skeleton.

Substrate-Binding Loop and the Core Region of the Enzymes of the SDR Family. As mentioned above (see Results), a large conformation change occurs upon substrate binding to 7α-HSDH. This change can be described as a swinging of the substrate-binding loop (residues 195−210) as a whole with the main-chain connections at Thr194 (N-terminal hinge) and Gln211 (C-terminal hinge) acting as the hinges. In the case of 3α,20β-HSDH (Ghosh et al., 1994b), however, only a small conformation change was noticed as occurring at the short α-helix located between the βF strand and the αG helix. As shown in Figure 6, this short helix is topologically equivalent to the αFG1 helix in 7α-HSDH which exhibited a large movement upon substrate binding. An equivalent short helix is also found in DHPR (Figure 6). Thus the hinge bending motion resulting in the displacement of a short helix between βF and αG is presumably a common feature occurring upon substrate binding among the enzymes belonging to the SDR family.

In this connection, it is intriguing to note the presence of two well-conserved proline residues (stressed in Figure 9) among the enzymes belonging to the SDR family. In the case of 7α-HSDH, these are Pro189, which is located five residues upstream from the N-terminal hinge (defined above), and Pro214, which is three residues downstream from the C-terminal hinge. These two Pro residues are shown in blue in Figure 10a. Thus the presence of these two Pro residues must be one of the devices to stabilize (through the rigidity of the main-chain segment involving a Pro residue) the region close to the hinges and thus to prevent the propagation of the effect of flexible loop movement into the core region (shown in white in Figure 10a), which may well spoil the normal binding mode of the cofactor (shown in pink in Figure 10a). This argument about the role of the conserved Pro residues appears to held for other members of the SDR family as well [confirmed by superimposing the crystal structures of these enzymes (data not shown)].

As seen in Figures 5 and 10a, the core region provides the right side and bottom surfaces of the active-site cleft, while the substrate-binding loop and a C-terminal segment provide the left side surface of the cleft. The cofactor molecule binds to the bottom surface, and the substrate molecule is almost stacked on top of the cofactor molecule (see Figure 10a). The present work shows that the substrate-binding loop is so designed as to make possible the large induced-fit movement upon substrate binding. It should also be noted that the structure of this loop is much more variable than those of other portions of the enzymes with respect to both primary and tertiary structures. Inspecting Figure 9, one sees that, for this loop and the C-terminal segment, even the lengths of the polypeptide chain segments are much varied among the enzymes of the SDR family. Thus it will be justified to describe the general architecture of these enzymes in the following way: (1) the tertiary structures of the core regions are conserved, despite considerable variability in their primary sequences, apparently to ensure the formation of part of the active-site cleft and a common binding mode of the cofactors, but (2) the lengths and conformations of the substrate-binding loop and the C-terminal segment are varied among these enzymes, apparently to accommodate distinct types of substrates in distinct orientations so as to expose the susceptible positions (such as position 7 of the steroid skeleton) in the substrate to the attacking catalytic groups (such as the hydroxyl group of Tyr159 in 7α-HSDH).

Other Single-Domain Oxidoreductases. Recently, we have been surprised at the similarity of the crystal structure of enoyl-acyl carrier protein reductase (called InhA) (Dessen et al., 1995) to the presently elucidated structure. The enzyme InhA is a drug targeting protein of *Mycobacterium* whose mutation yields a drug-resistant strain which causes mortality in 70−90% of AIDS-stricken patients who develop tuberculosis. Despite the fact that the primary structure of InhA shows no homology to that of the enzymes of the SDR family, the overall folding topology of InhA is completely identical with that of 7α-HSDH depicted in Figure 6a. The mode of interaction between the enzyme surface and the coenzyme NADH is also similar. Thus the basic folding topology of 7α-HSDH is not only shared by other enzymes of the SDR family but also most probably shared by other NAD(P)(H)-dependent single-domain oxidoreductases. The proteins folded in this way must be the smallest unit that could possess enzymatic activity using coenzyme NAD(P)(H).

Given this situation, the detailed knowledge of the structural features of 7α-HSDH may facilitate rational drug design targeting not only for the enzymes belonging to the SDR family, such as 11β-HSDH (controlling blood pressure), 17β-HSDH (implicated in breast cancer), and 15-hydroxyprostaglandin dehydrogenase (controlling biological activity of the prostaglandins), but also for other single-domain oxidoreductases, such as InhA (drug-targeting protein of *Mycobacterium*).

NOTE ADDED IN PROOF

After submission of this paper for publication, we solved the crystal structure of another enzyme of the SDR family, mouse lung carbonyl reductase (MLCR), as a ternary complex with NADPH and 2-propanol as a reaction product. The paper reporting this structure has already appeared (Tanaka et al., 1996b). This structure provided an intriguing clue as to the structural origin of NADH or NADPH preference exhibited by the enzymes of the SDR family.

Moreover, as demonstrated in Figure 9 of this paper, the equivalent disposition of the "Ser-Tyr-Lys triad" relative to the susceptible group of the product molecule was observed in both the ternary complex of 7α-HSDH (present study) and that of MLCR. Most notably, both of the side chains of the Ser and Tyr residues in the triad are directly hydrogen-bonded to the susceptible carbonyl oxygen in MLCR as well as in 7α-HSDH, suggesting the generality of the catalytic mechanism proposed in Figure 11 of the present paper among the enzymes of the SDR family.

ACKNOWLEDGMENT

The extensive comments raised by the referees and a member of Editorial Advisory Board have been extremely valuable for improving the manuscript. The Editor's patient effort is gratefully acknowledged. We thank Dr. T. Senda of the present group for crystallographic discussions. We thank Drs. M. Suzuki and N. Watanabe and Prof. N. Sakabe for help with data collection at the Photon Factory, Tsukuba, Japan. Our thanks are also due to Drs. M. Nakanishi and Y. Deyashiki and Prof. A. Hara at the Gifu Pharmaceutical University for stimulating discussions.

REFERENCES

Albalat, R., Duarte, G., & Atrian, S. (1992) *FEBS Lett. 165*, 190−196.

Al-Karadaghi, S., Cedergren-Zeppezauer, E. S., Hövmoller, S., Petratos, K., Terry, H., & Wilson, K. S. (1994) *Acta Crystallogr. D50*, 793−807.

Amuro, Y., Yamade, W., Yamamoto, T., Maebo, A., Hada, T., & Higashino, K. (1987) *Biochim. Biophys. Acta 917*, 101−107.

Baron, S. F., Franklund, C. V., & Hylemon, P. B. (1991) *J. Bacteriol. 173*, 4558−4569.

Birktoft, J. J., Rhodes, G., & Banaszak, L. J. (1989) *Biochemistry 28*, 6065−6081.

Brünger, A. T. (1992) *Nature 355*, 472−475.

Brünger, A. T., & Krukowski, A. (1990) *Acta Crystallogr. A46*, 585−593.

Brünger, A. T., Kuriyan, J., & Karplus, M. (1987) *Science 235*, 458−460.

Chen, Z., Jiang, J. C., Lin, Z. G., Lee, W. R., Baker, M. E., & Chang, S. H. (1993) *Biochemistry 32*, 3342−3346.

Collaborative Computational Project, Number 4 (1994) *Acta Crystallogr. D50*, 760−763.

Cols, N., Marfany, G., Atrian, S., & Gonzalez-Duarte, R. (1993) *FEBS Lett. 319*, 90−94.
Dessen, A., Quemard, A., Blanchard, J. S., Jacobs, W. R., Jr., & Sacchettini, J. C. (1995) *Science 267*, 1638−1641.
Ensor, C. M., & Tai, H. H. (1991) *Biochem. Biophys. Res. Commun. 176*, 840−845.
Franklund, C. V., Prada, P., & Hylemon, P. B. (1990) *J. Biol. Chem. 265*, 9842−9849.
Ghosh, D., Weeks, C. M., Grochulski, P., Duax, W. L., Erman, M., Rimsay, R. L., & Orr, J. C. (1991) *Proc. Natl. Acad. Sci. U.S.A. 88*, 10064−10068.
Ghosh, D., Wawrzak, Z., Weeks, C. M., Duax, W. L., & Erman, M. (1994a) *Structure 2*, 629−640.
Ghosh, D., Erman, M., Wawrzak, Z., Duax, W. L., & Pangborn, W. (1994b) *Structure 2*, 973−980.
Ghosh, D., Pletnev, V. Z., Zhu, D.-.W., Wawrzak, Z., Duax, W. L., Pangborn, W., Labrie, F., & Lin, S.-X. (1995) *Structure 3*, 503−513.
Harrison, D. H., Bohren, K. M., Ringe, D., Petsko, G. A., & Gabbay, K. H. (1994) *Biochemistry 33*, 2011−2020.
Higashi, T. (1989) *J. Appl. Crystallogr. 22*, 9−18.
Hylemon, P. B., & Sherrod, J. A. (1975) *J. Bacteriol. 122*, 418−424.
Inoue, T., Sunagawa, M., Mori, A., Imai, C., Fukuda, M., Takagi, M., & Yano, K. (1989) *J. Bacteriol. 171*, 3115−3122.
IUPAC−IUB Joint Commission on Biochemical Nomenclature (1983) *Eur. J. Biochem. 131*, 9−15.
Jörnvall, H., Persson, M., & Jeffery, J. (1981) *Proc. Natl. Acad. Sci. U.S.A. 78*, 4226−4230.
Jörnvall, H., Bahr-Lindstrom, H., Jany, K.-D., Ulmer, W., & Froschle, M. (1984) *FEBS Lett. 165*, 190−196.
Jörnvall, H., Persson, B., Krook, M., Atrian, S., Gonzalez-Duarte, R., Jeffery, J., & Ghosh, D. (1995) *Biochemistry 34*, 6003−6013.
Kabsch, W., & Sander, C. (1983) *Biopolymers 22*, 2577−2637.
Knight, S. (1989) Ph.D. Thesis, Swedish University of Agricultural Sciences, Uppsala, Sweden.
Kraulis, P. J. (1991) *J. Appl. Crystallogr. 24*, 946−950.
Laskowski, R. A., MacArthur, M. W., Moss, D. S., & Thorton, J. M. (1993) *J. Appl. Crystallogr. 26*, 283−291.
Lindley, P. F., Mahmoud, M. M., & Watson, F. E.(1980) *Acta Crystallogr. B36*, 1893−1897.
Luzzati, P. V. (1952) *Acta Crystallogr. 5*, 802−810.
Macdonald, I. A., Williams, C. N., & Mahony, D. E. (1973) *Biochim. Biophys. Acta 309*, 243−253.
Macdonald, I. A., Williams, C. N., Mahony, D. E., & Christie, W. M. (1975) *Biochim. Biophys. Acta 384*, 12−24.
Matthews, B. W. (1968) *J. Mol. Biol. 33*, 491−497.
Morris, A. L., MacArthur, M. W., Hutchinson, E. G., & Thornton, J. M. (1992) *Proteins: Struct., Funct., Genet. 12*, 345−364.
Obeid, J., & White, P. C. (1992) *Biochem. Biophys. Res. Commun. 188*, 222−227.
Orengo, C. A., Jones, D. T., & Thornton, J. M. (1994) *Nature 372*, 631−634.
Otwinoski, W. (1991) in *Proceedings of the CCP4 study weekend* (Wolf, W., Evans, P. R., & Leslie, A. G. W., Eds.) pp 80−86, SERC Daresbury Laboratory. Warrington, U.K.
Persson, B., Krook, M., & Jörnvall, H. (1991) *Eur. J. Biochem. 200*, 537−543.
Piontek, K., Chakrabarti, P., Schar, H.-P., Rossmann, M. G., & Zuber, H. (1990) *Proteins: Struct., Funct., Genet. 7*, 74−92.
Prabha, V., Gupta, M., & Gupta, K. G. (1989) *Can. J. Microbiol. 35*, 1076−1080.
Prabha, V., Gupta, M., Seiffge, D., & Gupta, K. G. (1990) *Can. J. Microbiol. 36*, 131−135.
Ramachandran, G. N., Ramakrishnan, C., & Sasisekharan, V. (1963) *J. Mol. Biol. 7*, 95−99.
Rossmann, M. G., Liljas, A., Branden, C.-I., & Banaszak, L. J. (1975) in *The Enzymes* (Boyer, P. D., Ed.) pp 61−102, Academic Press, New York.
Sakabe, N., Ikemizu, S., Sakabe, K., Higashi, T., Nakagawa, A., Watanabe, N., Adachi, S., & Sasaki, K. (1995) *Rev. Sci. Instrum. 66*, 1276−1281.
Sherrod, J. A., & Hylemon, P. B. (1977) *Biochim. Biophys. Acta 486*, 351−358.
Skarzynski, T., Moody, P. C. E., & Wonacotto, A. J. (1987) *J. Mol. Biol. 193*, 171−187.
Takeuchi, Y., Satow, Y., Nakamura, K. T., & Mitsui, Y. (1991) *J. Mol. Biol. 221*, 309−325.
Tanaka, N., Nonaka, T., Yoshimoto, T., Tsuru, D., & Mitsui, Y. (1996a) *Acta Crystallogr. D52*, 215−217.
Tanaka, N., Nonaka, T., Nakanishi, M., Deyashiki, Y., Hara, A., & Mitsui, Y. (1996b) *Structure 4*, 33−45.
Varughese, K. I., Skinner, M. M., Whiteley, J. M., Matthews, D. A., & Xuong, N. H. (1992) *Proc. Natl. Acad. Sci. U.S.A. 89*, 6080−6084.
Varughese, K. I., Xuong, N. H., Kiefer, P. M., Matthews, D. A., & Whiteley, J. M. (1994) *Proc. Natl. Acad. Sci. U.S.A. 91*, 5582−5586.
Whitely, J. M., Xuong, N. H., & Varughese, K. I. (1993) in *Chemistry and Biology of Pteridines and Folates* (Ayling, J. E., Nair, M. G., & Baugh, C. M. Eds.) pp 115−121, Plenum, New York.
Yoshimoto, T., Higashi, H., Kanatani, A., Xu, S. L., Nagai, H., Oyama, H., Kurazono, K., & Tsuru, D. (1991) *J. Bacteriol. 173*, 2173−2179.
Yoshimoto, T., Nagai, H., Ito, K., & Tsuru, D. (1993) *J. Bacteriol. 175*, 5730.
Zhang, K. Y. J. (1993) *Acta Crystallogr. D49*, 213−222.
Zhang, K. Y. J., & Main, P. (1990) *Acta Crystallogr. A46*, 41−46.

BI951904D